

An alternative cell cycle coordinates multiciliated cell differentiation

<https://doi.org/10.1038/s41586-024-07476-z>

Received: 19 April 2023

Accepted: 26 April 2024

Published online: 29 May 2024

 Check for updates

Semil P. Choksi¹✉, Lauren E. Byrnes¹, Mia J. Konjikusic¹, Benedict W. H. Tsai¹, Rachel Deleon¹, Quanlong Lu², Christopher J. Westlake² & Jeremy F. Reiter^{1,3}✉

The canonical mitotic cell cycle coordinates DNA replication, centriole duplication and cytokinesis to generate two cells from one¹. Some cells, such as mammalian trophoblast giant cells, use cell cycle variants like the endocycle to bypass mitosis². Differentiating multiciliated cells, found in the mammalian airway, brain ventricles and reproductive tract, are post-mitotic but generate hundreds of centrioles, each of which matures into a basal body and nucleates a motile cilium^{3,4}. Several cell cycle regulators have previously been implicated in specific steps of multiciliated cell differentiation^{5,6}. Here we show that differentiating multiciliated cells integrate cell cycle regulators into a new alternative cell cycle, which we refer to as the multiciliation cycle. The multiciliation cycle redeploys many canonical cell cycle regulators, including cyclin-dependent kinases (CDKs) and their cognate cyclins. For example, cyclin D1, CDK4 and CDK6, which are regulators of mitotic G1-to-S progression, are required to initiate multiciliated cell differentiation. The multiciliation cycle amplifies some aspects of the canonical cell cycle, such as centriole synthesis, and blocks others, such as DNA replication. E2F7, a transcriptional regulator of canonical S-to-G2 progression, is expressed at high levels during the multiciliation cycle. In the multiciliation cycle, E2F7 directly dampens the expression of genes encoding DNA replication machinery and terminates the S phase-like gene expression program. Loss of E2F7 causes aberrant acquisition of DNA synthesis in multiciliated cells and dysregulation of multiciliation cycle progression, which disrupts centriole maturation and ciliogenesis. We conclude that multiciliated cells use an alternative cell cycle that orchestrates differentiation instead of controlling proliferation.

Throughout the body, multiciliated cells propel overlying fluids^{4,7}. These cells are distinguished by their ability to generate as many as 500 centrioles, each of which serves as a basal body to template a motile cilium^{3,4,8}.

Multiciliated cells differentiate from precursors that progress through stages I–IV^{9–12} (Extended Data Fig. 1). Multiciliated cell precursors induce transcription factors such as MYB^{9,11,13,14}. During stage I, multiciliated cells express proteins required for centriole biogenesis¹⁵. During stage II, specialized structures called deuterosomes generate centrioles^{16,17}. During stage III, these centrioles disengage, migrate, mature into basal bodies and dock to the apical membrane. During stage IV, these basal bodies produce motile cilia (Extended Data Fig. 1). We investigated how cells orchestrate these complex steps to generate a functional multiciliated cell.

Most cells have two centrioles in the G1 phase of the mitotic cycle, duplicate their centrioles once and only once during S phase and distribute the four resulting centrioles equally to their daughters in mitosis^{18,19}. Multiciliated cells bypass the limits of regular centriole synthesis. Several regulators of the canonical cell cycle have been

previously linked to multiciliated cell differentiation^{5,6,20}. The mitotic oscillator, comprising CDK1 and anaphase-promoting complex/cyclosome (APC/C), directs centriole growth and disengagement⁵. CDK2 activity regulates both early stages of multiciliated cell differentiation and ciliogenesis⁶. In addition, multiciliated cell differentiation depends on cell-cycle-associated transcriptional regulators, such as E2F4, E2F5 and MYB^{9,13,21,22}. These parallels between the cell cycle and multiciliated cell differentiation led us to propose that an alternative cell-cycle-like program may participate in multiciliated cell development.

Multiciliated cells express cell cycle genes

To begin to test this hypothesis and to map transcriptional changes during multiciliated cell differentiation, we performed single-cell RNA sequencing (scRNA-seq) of differentiating mouse tracheal epithelial cells (mTECs). We combined cells differentiated by air–liquid interface culture for various lengths of time (Methods) to capture a range of differentiation stages. Marker gene and pseudotime analyses identified a differentiation trajectory initiating within basal stem cells, branching

¹Department of Biochemistry and Biophysics, Cardiovascular Research Institute, University of California, San Francisco, San Francisco, CA, USA. ²Laboratory of Cell and Developmental Signaling, Center for Cancer Research, National Cancer Institute, National Institutes of Health, Frederick, MD, USA. ³Chan Zuckerberg Biohub, San Francisco, CA, USA. [✉]e-mail: semil.choksi@ucsf.edu; jeremy.reiter@ucsf.edu

Article

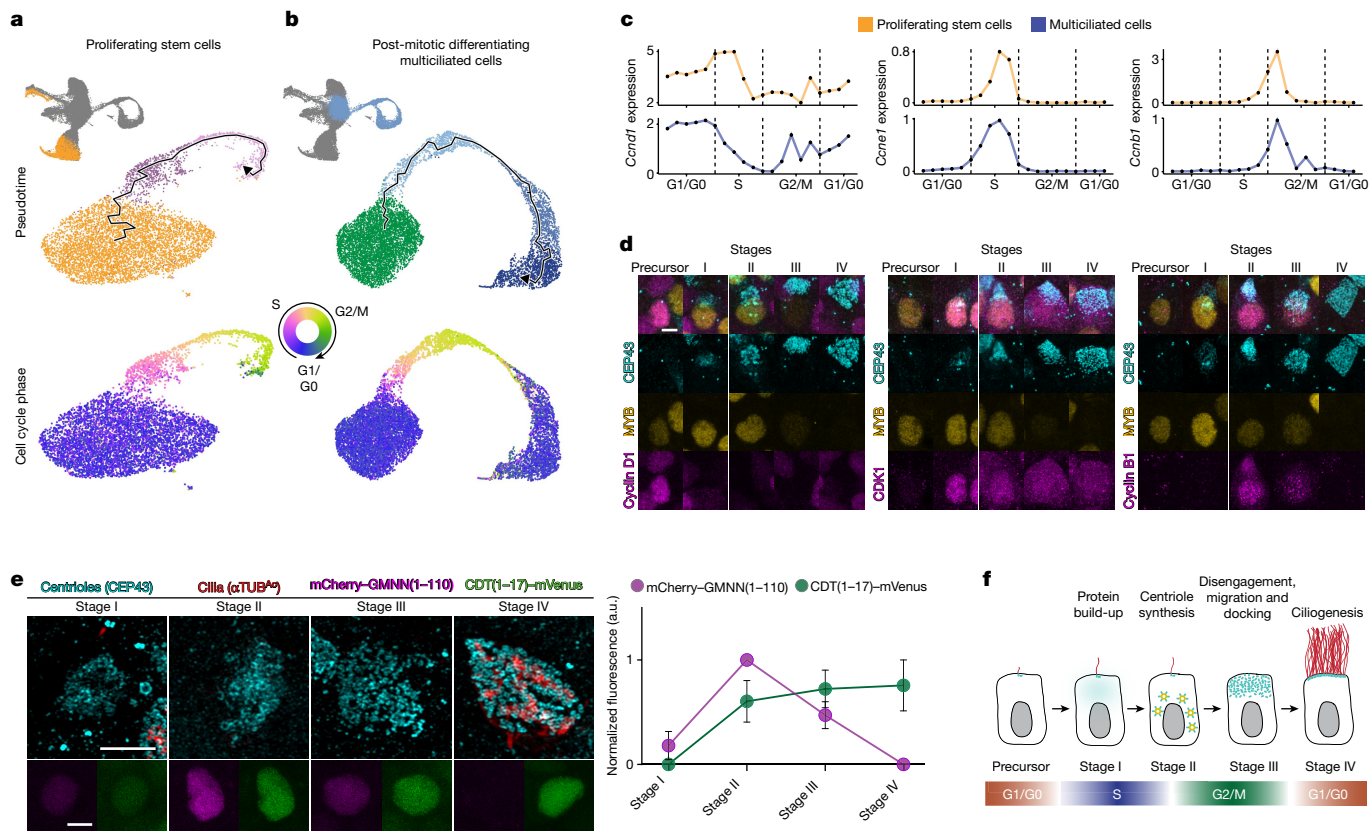


Fig. 1 | Differentiating post-mitotic multiciliated cells transit through a cell-cycle-like program. **a**, Cell cycle phase of basal stem cells. Insets show uniform manifold approximation and projection (UMAP) plots of the combined scRNA-seq data of differentiating mTECs, whereby orange indicates *Krt5*-expressing and *Trp63*-expressing basal stem cells selected for pseudotime analysis. Top, subclustered basal stem cells coloured by cluster identity. Bottom, cell cycle phase predicted by tricycle. Pseudotime infers a trajectory (arrow) corresponding to cell cycle phases. **b**, Identification of cycle phase of multiciliated cells. Blue in inset depicts *Gmnc*-expressing and *Foxj1*-expressing multiciliated cells selected for pseudotime analysis. Top, subclustered multiciliated cells coloured by cluster identity. Bottom, tricycle analysis reveals differentiating multiciliated cell expression reflective of G1/G0 (blue), S (pink) and G2/M phases (yellow-green). Pseudotime infers a trajectory (arrowhead) corresponding to progression from a G1/G0-like phase, through an S-like phase and a G2/M-like phase to a second G1/G0-like phase. **c**, Expression profiles of

Ccnd1, *Ccne1* and *Ccnb1* across cycle phases for basal stem cells and multiciliated cells. **d**, Representative immunofluorescence images of differentiating mTECs stained for centrioles (CEP43), an early multiciliated cell transcription factor (MYB) and cell cycle regulators cyclin D1 (left), CDK1 (centre) and cyclin B1 (right). $n = 3$ biological replicates. **e**, Left, immunofluorescence images of PIP-FUCCI mTECs stained for centrioles (CEP43) and cilia (acetylated tubulin (α TUB^{A_c})). Bottom panels depict mCherry-GMNN(1-110) (magenta) and CDT(1-17)-mVenus (green) native fluorescence. Stage based on centriole and cilia status. Right, quantification of nuclear mCherry-GMNN(1-110) fluorescence and nuclear CDT(1-17)-mVenus fluorescence, minimum and maximum normalized and plotted against the stage of multiciliated cell differentiation. Points are means of three biological replicates, with bars indicating \pm s.e.m. **f**, Multiciliated cell differentiation, divided into stages and corresponding phases of the multiciliation cycle. Scale bars, 5 μ m (d,e).

in intermediate cells and ending in differentiated multiciliated cells (Extended Data Fig. 2a–c and Supplementary Table 1), similar to those previously described for the upper airway^{11,20,23,24}. Intermediate cells, so called because of their intermediate position on the differentiation trajectory, contained the precursors that give rise to mature multiciliated cells¹¹. The multiciliated cell pseudotime trajectory reflected the stages of multiciliated cell differentiation¹¹ (Extended Data Fig. 2c,e).

Different phases of the canonical cell cycle exhibit distinct gene expression signatures²⁵. Analyses of basal stem cells (defined by *Krt5* expression) for cell-cycle-phase-dependent gene expression revealed that subsets of stem cells expressed genes reflective of the G1/G0, S and G2/M phases, consistent with their engagement in the canonical cell cycle (Fig. 1a and Extended Data Fig. 2d,f).

Although multiciliated cells are post-mitotic, we also analysed differentiating multiciliated cells for gene expression patterns indicative of cell cycle phases^{9,13}. Notably, cells early in the multiciliated lineage expressed genes reflective of a G1/G0 phase (Fig. 1b and Extended Data Fig. 3). As multiciliated cells differentiated, they expressed genes reflective of S phase and, later, genes reflective of G2/M phase (Fig. 1b and

Extended Data Fig. 2e,f). Mature multiciliated cells displayed gene expression patterns reflective of a second G1/G0-like phase (Fig. 1b and Extended Data Fig. 3). For example, cyclins associated with G1, S and G2/M phases were expressed successively across these phases of multiciliated cell differentiation (Fig. 1c and Extended Data Fig. 3). Thus, differentiating multiciliated cells exhibit a cell-cycle-like transcriptional program.

To establish whether the cell-cycle-like transcriptional program is reflected at the protein level, we examined differentiating mTECs for cell cycle regulator proteins at different stages of multiciliated cell differentiation, defined by MYB expression and centriole morphology. Cyclin D1 was expressed in multiciliated cell precursors and then down-regulated during differentiation (Fig. 1d). CDK1 localized to the nucleus in stage I multiciliated cells and then became cytoplasmic as multiciliated cells matured (Fig. 1d). Cyclin B1 was expressed in stages II and III of differentiating multiciliated cells (Fig. 1d). The dynamic expression and localization of these cell cycle regulators suggested that they may coordinate the stages of multiciliated cell differentiation.

To begin to test this possibility, we transduced differentiating mTECs with a reporter of cell cycle activity: the PIP-degron-containing

fluorescent ubiquitination-based cell cycle indicator PIP–FUCCI²⁶. PIP–FUCCI uses two fluorescent reporters, CDT1(1–17)–mVenus and mCherry–GMNN(1–110), which are degraded at different phases of the cell cycle. In proliferating cells, mCherry fluorescence without mVenus indicates S phase, whereas high levels of both mCherry and mVenus are associated with G2/M, and mVenus with no mCherry expression indicates G1/G0 phase²⁶. In multiciliated cells, PIP–FUCCI fluorescence levels were dynamic across the stages of differentiation (Fig. 1e). Stage I multiciliated cells exhibited some mCherry expression with low levels of mVenus. Stages II and III multiciliated cells showed increased mVenus and mCherry levels. Stage IV multiciliated cells maintained high mVenus levels but no mCherry (Fig. 1e).

Together, these data suggest that multiciliated cells display hallmarks of cell cycle progression during post-mitotic differentiation (Fig. 1f and Supplementary Table 2). The multiciliated cell precursors exhibited characteristics of G1/G0, including expression of *Ccnd1* (which encodes cyclin D1) and of *Cdk4* and *Cdk6* (*Cdk4/6*) (Extended Data Fig. 3). The stage I and early-stage II multiciliated cells displayed hallmarks of S phase, including *Cdk1* and *Ccne1* (which encodes the S phase regulator cyclin E1) expression. Late-stage II and stage III multiciliated cells were similar to cells in G2/M, expressing cyclin B1 and both PIP–FUCCI reporter proteins. Stage IV multiciliated cells returned to a second G1/G0-like phase, exemplified by *Cdk4/6* expression and high PIP–FUCCI mVenus-to-mCherry ratios. We call this cell-cycle-like progression during multiciliated cell differentiation the multiciliation cycle.

To evaluate proliferation in differentiating multiciliated cells, we assessed mTECs for ethynyl-2'-deoxyuridine (EdU) incorporation. Few differentiating multiciliated cells (marked by FOXJ1 expression²⁷) exhibited signs of DNA synthesis (Extended Data Fig. 4a,b). Assessment of mTECs for a marker of mitosis, phosphorylated histone H3 (H3S10P), revealed a sharp decline in the number of mitotic cells at the time of differentiation initiation (Extended Data Fig. 4c–e). These results confirm previous studies showing that multiciliated cells do not proliferate during differentiation^{9,13}. Therefore, we hypothesized that multiciliated cells use a modified cell cycle not for generating daughter cells but to regulate differentiation.

CDK4/6 initiate the multiciliation cycle

Ccnd1 and *Cdk4/6* were expressed in multiciliated cell precursors (Figs. 1c,d and 2a). During the canonical cell cycle, D-type cyclins activate CDK4/6 to direct the progression from early G1/G0 into S phase^{28–30}. To test whether these cell cycle regulators function in multiciliated cell differentiation, we treated mTECs with inhibitors of CDK4/6, palbociclib and ribociclib³¹. Inhibiting CDK4/6 activity during mTEC differentiation blocked centriole synthesis and ciliogenesis (Fig. 2b,d and Extended Data Fig. 5a,b). To determine whether the effect of CDK4/6 inhibition was specific to differentiation, we assessed cell density and found no change in palbociclib-treated or ribociclib-treated mTECs relative to vehicle control across these treatment regimens (Extended Data Fig. 5c). To assess how CDK4/6 activity promotes multiciliated cell differentiation, we examined the expression of early multiciliated cell transcription factors, MYB and FOXJ1, in CDK4/6 inhibited cells. CDK4/6 activity was required for MYB and FOXJ1 expression, which suggests that CDK4/6 activity may be required early in multiciliated cell differentiation (Fig. 2c,e).

To further investigate the time at which CDK4/6 activity is required during multiciliated cell differentiation, we compared the scRNA-seq profiles of mTECs treated with ribociclib or vehicle control (DMSO) (Extended Data Fig. 5d–h). Marker gene analysis identified the major airway cell types and confirmed that CDK4/6 inhibition decreased the differentiation of multiciliated cells (Fig. 2f,g and Supplementary Table 3). CDK4/6 inhibition did not affect the proportion of other cell types, such as intermediate cells, which contain multiciliated cell precursors¹¹ (Fig. 2f,g and Extended Data Fig. 5d–h).

However, inhibiting CDK4/6 activity altered gene expression in intermediate cells. That is, CDK4/6 inhibition reduced the expression of several important transcriptional effectors of early multiciliated cell differentiation (for example, *Gmnc*, *Mycl*, *Myb* and *Foxj1*; Fig. 2h,i and Supplementary Table 4). These results further suggest that CDK4/6 activity is required for initiating multiciliated cell differentiation.

CDK4/6 activity also promoted the multiciliated cell expression of *Ccne1* (Fig. 2i). Therefore, we proposed that CDK4/6 drives progression from the G1/G0-like to the S-like phase of the multiciliation cycle. To test this hypothesis, we compared the cell cycle gene expression profiles of multiciliated cells treated with ribociclib or DMSO. CDK4/6 inhibition reduced the proportion of cells in the S-like phase of the multiciliation cycle (Fig. 2j,k). Thus, CDK4/6 activity is important for progression from the G1/G0-like phase to the S-like phase of the multiciliation cycle.

To test whether CDK4/6 activity is sufficient to drive multiciliated cell differentiation, we overexpressed a GFP-tagged cognate cyclin for CDK4/6, cyclin D1, in mTECs. Cyclin D1–GFP increased the proportion of multiciliated cells (Fig. 2l,m). These additional multiciliated cells differentiated with kinetics comparable to control multiciliated cells (Extended Data Fig. 5i,j). Therefore, cyclin D1–CDK4/6 drives the progression of cells from the G1/G0-like to the S-like phase of the multiciliation cycle to initiate multiciliated cell-specific gene expression and multiciliated cell differentiation (Fig. 2n).

The multiciliation cycle is a variant cell cycle

To begin to discern what distinguishes the multiciliation cycle, we compared expression profiles between multiciliated cells and proliferating stem cells. The expression of many cell cycle genes was dampened during the multiciliation cycle relative to the canonical cell cycle (Fig. 3a, Extended Data Fig. 6a,b and Supplementary Table 2). For example, S phase genes encoding DNA replication regulators, such as *Gmnn*, *Mcm5* and *Gins2*, were expressed at lower levels in the multiciliation cycle than in the cell cycle (Fig. 3a). Similarly, expression of G2/M phase-associated genes encoding the central spindle complex, important for chromosome segregation and cytokinesis (for example, *Kif23*, *Racgap1* and *Ect2*)³², were expressed at lower levels during the multiciliation cycle than the cell cycle (Fig. 3a).

To identify candidate multiciliation cycle regulators, we identified genes expressed at higher levels during the multiciliation cycle than during the canonical cell cycle. As expected, multiciliated cells preferentially expressed genes encoding regulators of centriole synthesis, including *Plk4*, *Sass6* and *Deup1* (Extended Data Fig. 6c). In addition, we identified several cell cycle regulators enriched in the multiciliation cycle, including *Ccno* (which encodes a noncanonical cyclin previously implicated in multiciliated cell differentiation³³), *Cdkn1a* (which encodes the CDK inhibitor p21^{CIP1}) and *E2f7* (Fig. 3a, Extended Data Fig. 6d).

E2f7 encodes an atypical repressor in the E2F transcription factor family that represses S phase gene expression to promote the transition from the S to G2 phase in proliferating cells^{34,35}. We proposed that E2F7 may also regulate progression through the multiciliation cycle. E2F7 was upregulated specifically in mouse adult tracheal cells undergoing centriole synthesis (Fig. 3b). Similarly, E2F7 was expressed transiently during stages I and II of mTEC multiciliated cell differentiation (Fig. 3c). As stages I and II correspond to S-like and early G2/M-like phases of the multiciliation cycle and as E2F7 promotes the transition from S to G2 in proliferating cells^{34,35}, we speculated that E2F7 terminates the S-like phase of the multiciliation cycle.

E2F7 advances the multiciliation cycle

To investigate the role of E2F7 in the multiciliation cycle, we generated mice with mutated *E2f7* (Extended Data Fig. 6e). *E2f7*^{−/−} mice were

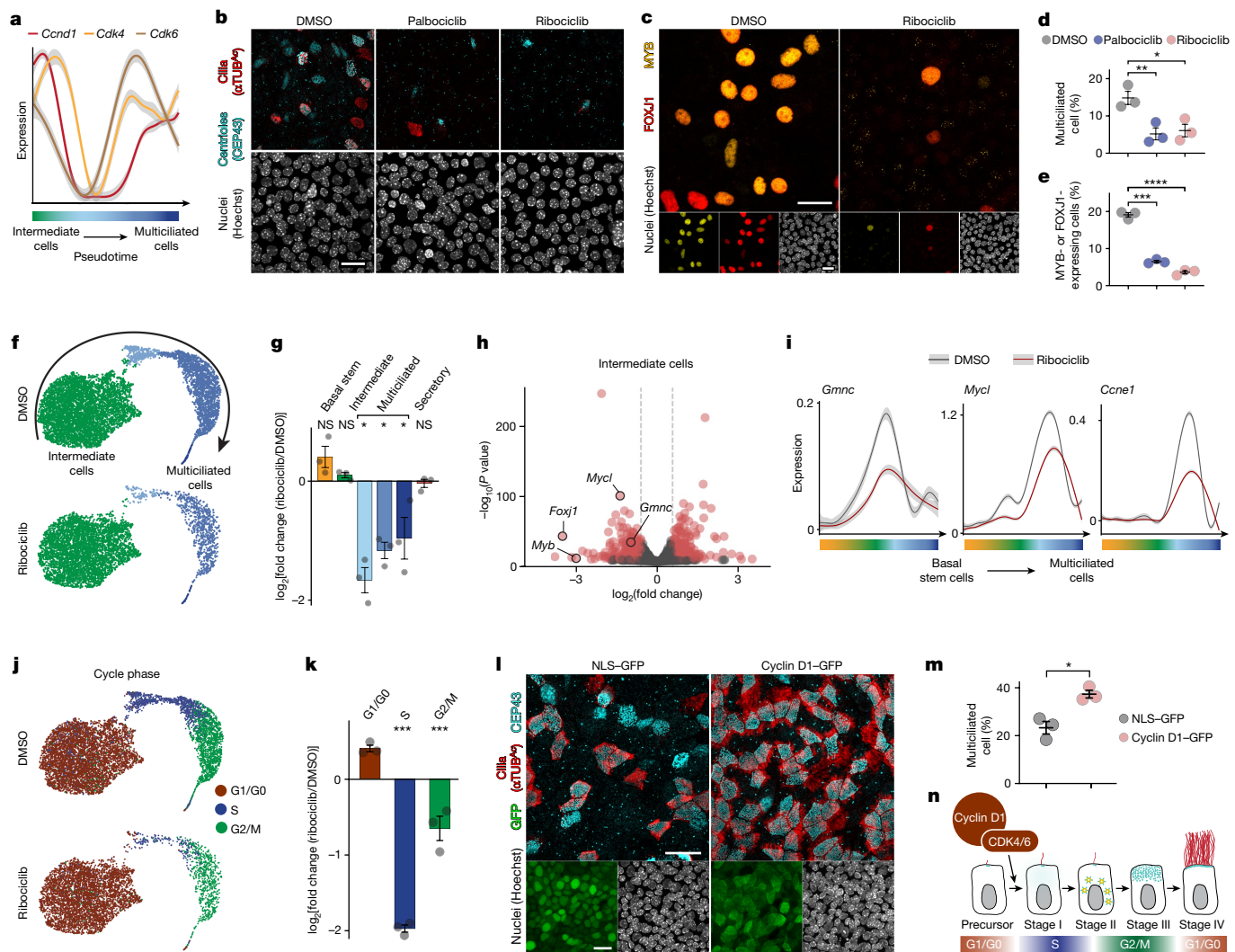


Fig. 2 | Cyclin D1–CDK4/6 initiates multiciliated cell differentiation. **a**, Minimum and maximum normalized scRNA-seq expression across multiciliated cell differentiation pseudotime. Grey bars indicate 95% confidence intervals. Coloured x-axis indicates cluster identity. **b**, mTECs treated with DMSO, palbociclib or ribociclib and stained for centrioles (CEP43), cilia (α TUB A) and nuclei. **c**, mTECs treated with DMSO or ribociclib and stained for MYB, FOXJ1 and nuclei. **d**, Percentage of multiciliated cells after DMSO, palbociclib or ribociclib treatment. Horizontal lines indicate means \pm s.e.m. of 3 biological replicates, ** P = 0.0118, * P = 0.0183 (one-way analysis of variance (ANOVA) with Dunnett's correction). **e**, Percentage of MYB-expressing or FOXJ1-expressing cells after DMSO, palbociclib or ribociclib treatment. Horizontal lines indicate means \pm s.e.m. of 3 biological replicates, *** P = 0.000002, **** P = 0.0000007 (one-way ANOVA with Dunnett's correction). **f**, scRNA-seq UMAP of mTEC intermediate and differentiating multiciliated cells after DMSO or ribociclib treatment. Arrow indicates differentiation trajectory. **g**, Change in cell cluster proportion after ribociclib treatment. Bars indicate means \pm s.e.m. of 3 biological replicates, *false discovery rate (FDR) < 0.02 (two-tailed Bayes

quasi-likelihood F-test with Benjamini–Hochberg correction). **h**, Genes differentially expressed by ribociclib-treated intermediate cells compared with DMSO-treated cells. Red, fold-change > 1.5 and P < 0.0005 (two-tailed Wald test with Benjamini–Hochberg correction). **i**, scRNA-seq expression across multiciliated cell differentiation pseudotime (DMSO or ribociclib). Grey bars indicate 95% confidence intervals. Colours indicate cluster identity. **j**, scRNA-seq UMAP of tricycle-based cycle phase after DMSO or ribociclib treatment. **k**, Change in cycle phase proportion after ribociclib treatment. Bars indicate means \pm s.e.m. of 3 biological replicates, ***log₂(fold-change) < -0.5 and FDR < 0.0008 (two-tailed moderated t-test with Benjamini–Hochberg correction). **l**, mTECs expressing NLS–GFP or cyclin D1–GFP stained for centrioles (CEP43) and cilia (α TUB A). Bottom panels show GFP and nuclei staining. **m**, Proportion of multiciliated cells after cyclin D1–GFP expression. Horizontal lines indicate means \pm s.e.m. of 3 biological replicates, * P = 0.0102 (unpaired two-tailed t-test). **n**, Cyclin D1–CDK4/6 promotes the transition of precursor cells from the G1/G0-like phase to S-like phase of the multiciliation cycle. Scale bars, 10 μ m (b,c,l).

viable, as previously reported³⁵, and mTECs generated from mutant mice did not produce detectable levels of wild-type *E2f7* transcripts (Extended Data Fig. 6f,g). Both *E2f7*^{-/-} mTECs and trachea exhibited attenuated E2F7 protein (Extended Data Fig. 6h–j). To identify genes regulated by E2F7 in multiciliated cells, we analysed mTECs from *E2f7*^{-/-} and littermate controls using scRNA-seq (Extended Data Fig. 7a–g and Supplementary Table 5). We observed no alteration in the expression of multiciliated cell transcription factors or genes involved in centriole synthesis or ciliogenesis (Fig. 3d and Supplementary Table 6). Instead,

many genes encoding regulators of DNA replication were upregulated in stages II and III *E2f7*^{-/-} multiciliated cells (Fig. 3e, Extended Data Figs. 7h,i and 8a and Supplementary Table 7). For example, genes encoding DNA replication machinery, which were expressed at low levels in the multiciliation cycle (for example, *Mcm5* and *Gins2*; Fig. 3a), were derepressed in multiciliated cells lacking E2F7 (Fig. 3e,f). We conclude that in the multiciliation cycle, E2F7 restricts the expression of genes expressed during the late G1 and S phases of the canonical cell cycle (Extended Data Fig. 8a).

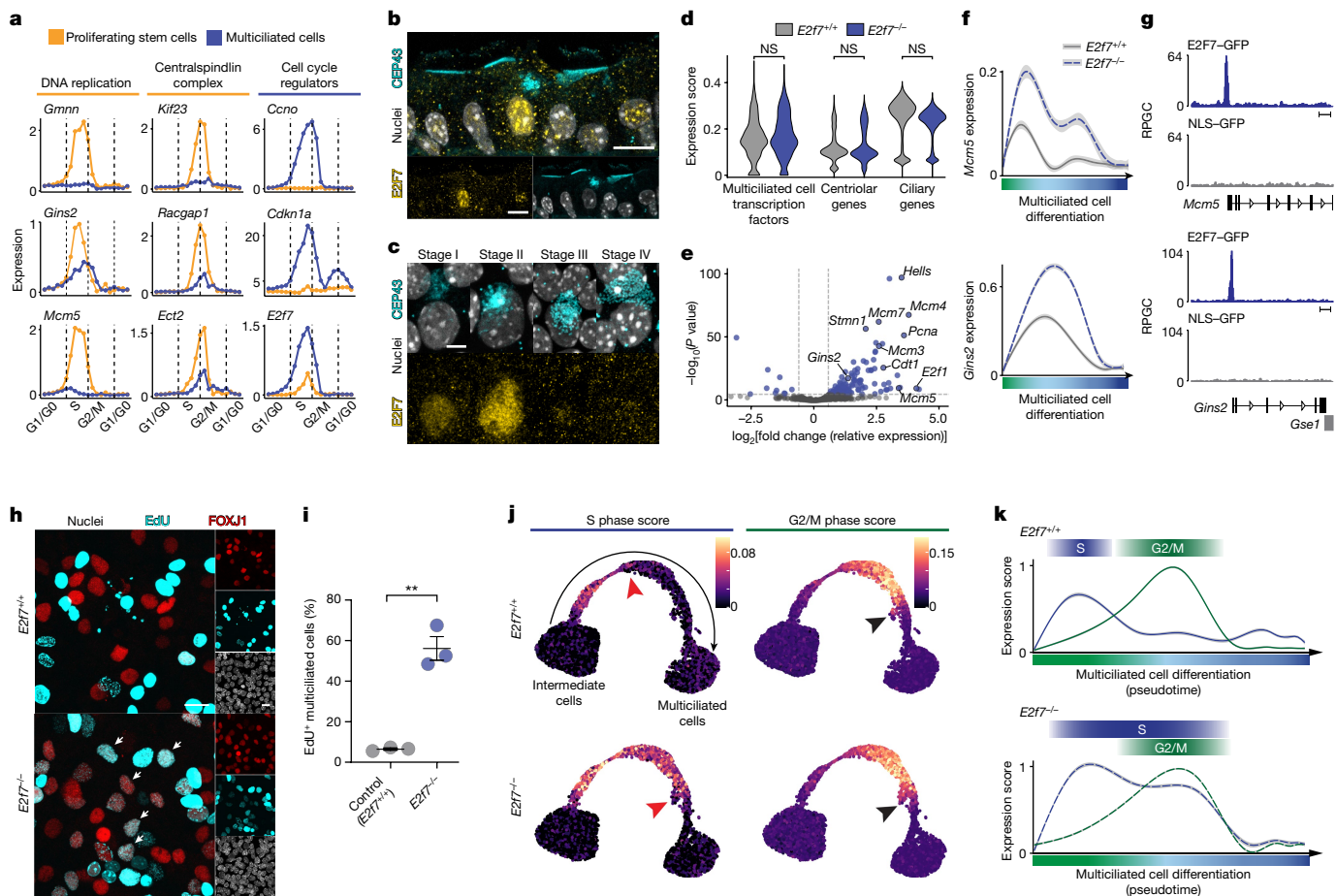


Fig. 3 | E2F7 blocks DNA replication and promotes progression through the multiciliation cycle. **a**, Average read counts across cycle phase of stem (orange) and multiciliated (blue) cells from the wild-type scRNA-seq dataset (Fig. 1). **b**, Representative image of adult mouse trachea immunostained for E2F7, centrioles (CEP43) and nuclei. $n = 3$ mice. **c**, mTECs immunostained for E2F7, centrioles (CEP43) and nuclei. Cells representative of each stage from three biological replicates are shown. **d**, Composite expression of multiciliated cell transcription factors, centriolar and ciliary genes in $E2f7^{+/+}$ and $E2f7^{-/-}$ multiciliated cells. Scores are the normalized Mann–Whitney U -statistic of gene set expression. NS, not significant (multiple unpaired two-tailed t -tests with Holm–Sidak correction). **e**, Genes differentially expressed between $E2f7^{-/-}$ and $E2f7^{+/+}$ differentiating multiciliated cells. Blue, fold-change >1.5 and $P < 0.00001$ (two-tailed Wald test with Benjamini–Hochberg correction). **f**, scRNA-seq expression in $E2f7^{+/+}$ and $E2f7^{-/-}$ multiciliated cells across pseudotime. Grey bars indicate 95% confidence intervals. **g**, E2F7-GFP or

NLS-GFP CUT&RUN in mTECs, presented as reads per genomic content (RPGC). **h**, $E2f7^{+/+}$ and $E2f7^{-/-}$ mTECs stained for EdU and FOXJ1. White arrows indicate $E2f7^{-/-}$ cells that express FOXJ1 and are EdU-positive. **i**, Percentage of $E2f7^{+/+}$ and $E2f7^{-/-}$ mTECs expressing FOXJ1 that are EdU-positive. Horizontal lines indicate means \pm s.e.m. of 3 biological replicates, $**P = 0.001$ (unpaired two-tailed t -test). **j**, S phase (left) and G2/M phase (right) gene signature scores derived from normalized sum rank of gene sets projected onto UMAPs of $E2f7^{+/+}$ and $E2f7^{-/-}$ multiciliated cells. Colours indicate expression score of S or G2/M gene sets. Arrow indicates differentiation trajectory. Red and black arrowheads indicate the end of the S and G2/M phases, respectively, as defined by the half-maximal phase score. **k**, $E2f7^{+/+}$ and $E2f7^{-/-}$ multiciliated cell minimum and maximum normalized S phase and G2/M phase gene signature scores across pseudotime. Grey bars indicate 95% confidence intervals. Scale bars, 10 μ m (**b**, **h**), 5 μ m (**c**) or 1 kb (**g**).

To identify which genes E2F7 might directly regulate in the multiciliation cycle, we determined where E2F7-GFP binds the genome in mTECs using cleavage under targets and release using nuclease (CUT&RUN)³⁶. E2F7-GFP bound near genes encoding DNA replication machinery, including *Mcm5* and *Gins2* (Fig. 3g, Extended Data Fig. 8a–c and Supplementary Table 8), which suggested that E2F7 directly represses DNA replication-related genes during the multiciliation cycle S-like phase. Comparing E2F7 target genes in mTECs to previously identified E2F7 target genes in proliferating cells revealed partial overlap, which indicated that E2F7 regulates a similar set of genes in the multiciliation cycle and the canonical cell cycle (Extended Data Fig. 8d,e and Supplementary Table 9).

A key difference between the cell cycle S phase and the multiciliation cycle S-like phase was DNA synthesis (Extended Data Fig. 4a,b). We proposed that increased expression of E2F7 in multiciliated cells may be responsible for this difference. To test this hypothesis, we performed EdU labelling of differentiating $E2f7^{-/-}$ and $E2f7^{+/+}$ mTECs. As expected,

few $E2f7^{+/+}$ multiciliated cells showed EdU incorporation (Fig. 3h,i). By contrast, $E2f7^{-/-}$ mTECs showed an 8.7-fold increase in the percentage of multiciliated cells incorporating EdU (Fig. 3h,i). Thus, E2F7 restricts DNA replication gene expression to repress DNA synthesis during the multiciliation cycle, and loss of E2F7 restores aspects of the canonical cell cycle to the multiciliation cycle.

Proliferating cells display a sharp cessation of S phase gene expression at the transition from S phase to G2/M phase³⁷. Similarly, wild-type differentiating multiciliated cells displayed a sharp cessation of S-like phase gene expression before the initiation of G2/M-like gene expression (Fig. 3j,k). In addition to increased levels of S phase gene expression, differentiating $E2f7^{-/-}$ multiciliated cells displayed delayed termination of S phase gene expression (Fig. 3j,k). By contrast, the timing of G2/M phase-related gene expression was unaffected in differentiating $E2f7^{-/-}$ multiciliated cells (Fig. 3j,k). Thus, without E2F7, differentiating multiciliated cells aberrantly express S-like and G2/M phase gene programs simultaneously. This overlap of S-like and

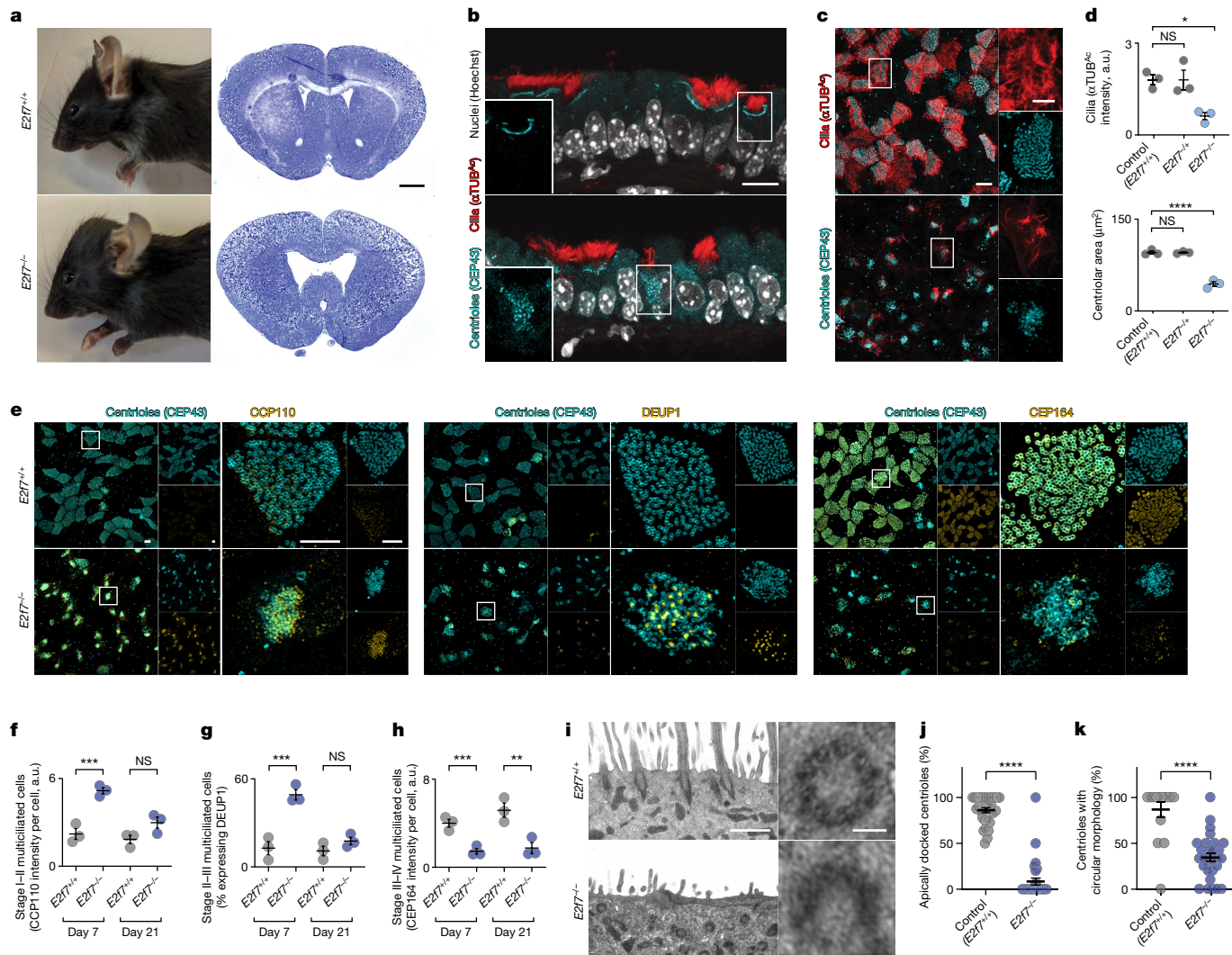


Fig. 4 | E2F7 coordinates centriole synthesis during multiciliated cell differentiation. **a**, Images of $E2f7^{+/+}$ and $E2f7^{-/-}$ littermate mice, with coronal brain sections stained with haematoxylin and eosin. Scale bar, 1 mm. **b**, Representative images of trachea immunostained for centrioles (CEP43), cilia (α TUB^{A_c) and nuclei. Insets show magnification of centrioles in boxed cells. $n = 3$ mice per genotype. Scale bar, 10 μ m. **c**, Left, mTECs immunostained for centrioles (CEP43) and cilia (α TUB^{A_c). Scale bar, 10 μ m. Right, magnifications of boxed cells. Scale bar, 5 μ m. **d**, Quantification of ciliary intensity (α TUB^{A_c) and centriolar area in mTECs. Horizontal lines indicate means \pm s.e.m. of 3 biological replicates, * $P = 0.0148$, *** $P = 0.000017$ (one-way ANOVA with Dunnett's correction). **e**, Left, mTECs immunostained for centrioles (CEP43) and CCP110 (left), deuterosomes (DEUP1, centre) and distal appendages (CEP164, right) after 7 days of differentiation. Right, magnifications of boxed cells, with individual channels in small panels. Scale bars, 5 μ m. **f**, Intensities of CCP110 immunofluorescence per multiciliated cell after 7 or 21 days. Horizontal lines indicate means \pm s.e.m. of 3 biological replicates, *** $P = 0.0004$, NS indicates}}}

$P = 0.0689$ (one-way ANOVA with Sidak's correction). **g**, Percentage of multiciliated cells possessing DEUP1-containing deuterosomes after 7 or 21 days. Horizontal lines indicate means \pm s.e.m. of 3 biological replicates, *** $P = 0.0002$, NS indicates $P = 0.3808$ (one-way ANOVA with Sidak's correction). **h**, Intensities of CEP164 immunofluorescence per multiciliated cell after 7 or 21 days. Horizontal lines indicate means \pm s.e.m. of 3 biological replicates, *** $P = 0.0088$, ** $P = 0.0015$ (one-way ANOVA with Sidak's correction). **i**, Left, transmission electron micrographs (TEMs) of multiciliated cells. Scale bar, 1 μ m. Right, undocked centrioles. Scale bar, 100 nm. **j**, Percentage of apically docked centrioles in TEMs of multiciliated cells. Horizontal lines indicate means \pm s.e.m. of 30 $E2f7^{+/+}$ cells (234 centrioles) or 30 $E2f7^{-/-}$ cells (212 centrioles), *** $P < 0.00000001$ (unpaired two-tailed t -test). **k**, Percentage of undocked centrioles that are circular in TEMs of multiciliated cells. Horizontal lines indicate means \pm s.e.m. of 18 $E2f7^{+/+}$ cells (37 undocked centrioles) or 29 $E2f7^{-/-}$ cells (199 undocked centrioles), *** $P = 0.00000001$ (unpaired two-tailed t -test).

G2/M-like phases in $E2f7^{-/-}$ multiciliated cells indicates that E2F7 helps enforce the transition from the S-like phase to the G2/M-like phase of the multiciliation cycle.

Multiciliated cell differentiation requires E2F7

$E2f7^{-/-}$ mice exhibited hydrocephalus (Fig. 4a and Extended Data Fig. 9a,b), a condition that can be caused by defective multiciliated ependymal cells in the brain³⁸. In $E2f7^{-/-}$ brain ventricles, oviducts and airways, multiciliated cells exhibited fewer cilia and increased

numbers of cytoplasmic, undocked centrioles (Fig. 4b and Extended Data Fig. 9c–g). Similarly, $E2f7^{-/-}$ mTECs showed fewer cilia per cell and clustered, undocked centrioles (Fig. 4c,d). These results suggested that E2F7 is crucial for multiciliated cell maturation. Several genes encoding cytoskeletal regulators were dysregulated in $E2f7^{-/-}$ multiciliated cells (Extended Data Fig. 8a) and therefore may contribute to centriole docking defects in cells lacking E2F7.

In the canonical cell cycle, E2F7 and a parologue, E2F8, have overlapping functions³⁵. In differentiating multiciliated cells, E2F8 was expressed and became further upregulated in $E2f7^{-/-}$ multiciliated

cells (Extended Data Fig. 10a–c). To assess whether *E2f8* regulates multiciliated cell differentiation, we used CRISPR–Cas9 to generate mTECs lacking *E2f8* (Extended Data Fig. 10d,e). *E2f8^{sgRNA}* multiciliated cells did not exhibit defects in differentiation or multiciliation (Extended Data Fig. 10f–i). *E2f7^{-/-}*–*E2f8^{sgRNA}* multiciliated cells exhibited defects in differentiation and multiciliation comparable with those of *E2f7^{-/-}* multiciliated cells (Extended Data Fig. 10f–i). These data suggest that *E2f8* is dispensable for multiciliated cell differentiation.

We sought to understand how the discoordination of the multiciliation cycle disrupts multiciliated cell differentiation by examining mTECs from *E2f7^{-/-}* mice and control littermates at 7 days of air–liquid interface culture. We examined the expression of proteins associated with each stage of multiciliated cell differentiation (Extended Data Fig. 1).

CCP110 caps newly synthesized centrioles and is removed before centriole maturation and ciliogenesis³⁹. During multiciliated cell differentiation, *CCP110* is removed from centrioles by stage III (Extended Data Fig. 1a). Assessing *E2f7^{-/-}* and control mTECs revealed that *CCP110* persisted on the centrioles of differentiating *E2f7^{-/-}* multiciliated cells (Fig. 4e,f).

Deuterosomes are present specifically during stages II and III of multiciliated cell differentiation (Extended Data Fig. 1b). Examining *E2f7^{-/-}* and control mTECs for *DEUP1*, a deuterosome component¹⁶, revealed that differentiating *E2f7^{-/-}* multiciliated cells exhibited persistent deuterosomes (Fig. 4e,g).

By stage IV, multiciliated cell centrioles have acquired distal appendages through which they dock to the apical membrane⁴⁰ (Extended Data Fig. 1c). Examining *E2f7^{-/-}* and control mTECs for *CEP164*, a distal appendage component, revealed that differentiating *E2f7^{-/-}* multiciliated cells were defective in recruiting *CEP164* (Fig. 4e,h).

Thus, after 7 days of air–liquid interface culture (a time point at which most *E2f7^{+/+}* multiciliated cells have progressed to stage IV), *E2f7^{-/-}* multiciliated cells were in stages II and III. To assess whether *E2f7^{-/-}* multiciliated cells were delayed in their differentiation, we repeated the analysis after air–liquid interface culture for 21 days. At this late time point, *E2f7^{-/-}* multiciliated cells had removed *CCP110* and deuterosomes, but still had not recruited *CEP164* (Fig. 4f–h), which indicated that *E2f7* promotes advancement from the multiciliated S-like phase to the G2/M-like phase. Moreover, in the absence of *E2f7*, dysregulation of this advancement disrupts the centriolar maturation essential for generating motile cilia.

To better understand how *E2f7* is required for the differentiation of mTECs, we used transmission electron microscopy to examine *E2f7^{-/-}* and *E2f7^{+/+}* mTECs cultured by the air–liquid method for 7 days. *E2f7^{+/+}* multiciliated cells displayed abundant docked centrioles with associated cilia (Fig. 4i,j). By contrast, multiciliated cells lacking *E2f7* displayed undocked centrioles and decreased ciliogenesis (Fig. 4i,j), consistent with defects in centriole maturation. Furthermore, many centrioles in multiciliated cells lacking *E2f7* were short or incomplete (Fig. 4i,k), which suggested that centriole synthesis is also disrupted in cells lacking *E2f7*.

Together, these data indicate that *E2f7* is required for the coordinated progression from the multiciliation cycle S-like phase into the G2/M-like phase. Termination of the S-like phase program is necessary for the timely execution of specific steps of multiciliated cell differentiation (for example, *CCP110* removal and deuterosome disassembly), without which later steps (for example, centriole maturation and ciliogenesis) are compromised.

Discussion

Several cell cycle regulators have previously been implicated in post-mitotic differentiating multiciliated cells^{5,6}. We report an alternative version of the cell cycle, the multiciliation cycle, which coordinates

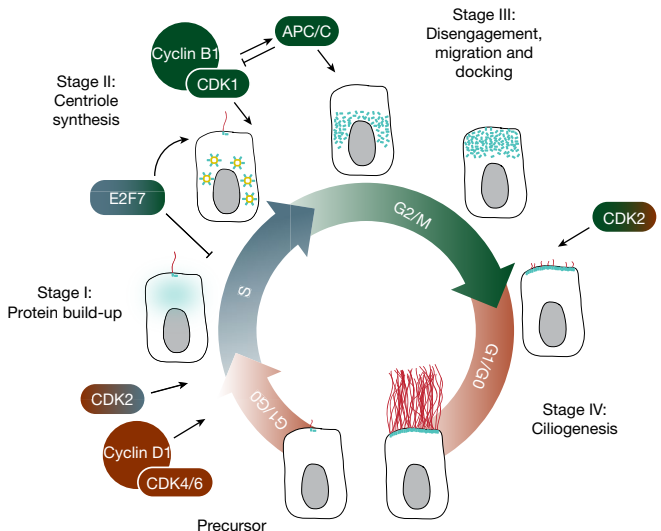


Fig. 5 | The multiciliation cycle is a cell cycle variant that coordinates differentiation. A model of how the multiciliation cycle coordinates multiciliated cell differentiation. Multiciliated cell precursors initiate differentiation in a G1/G0-like phase. Precursors progress into an S-like phase encompassing stage I and early stage II. Cyclin D1–CDK4/6 and CDK2 regulate entry into the S-like phase (this work and ref. 6). E2F7 suppresses DNA synthesis during the S-like phase and promotes the S-like to G2/M-like transition. During the G2/M-like phase, cyclin B1–CDK1 promotes the growth of newly forming centrioles and APC/C controls centriole number and progression to stage III of multiciliated cell differentiation, when centrioles dock to the membrane⁵. From the G2/M-like phase, differentiating multiciliated cells transition into the G1/G0-like phase corresponding to stage IV, ciliogenesis. CDK2 promotes this final stage of multiciliated cell differentiation⁶.

multiciliated cell differentiation to generate several hundred centrioles that mature into basal bodies and produce motile cilia (Fig. 5).

Like the canonical cell cycle, the multiciliation cycle involves the sequential expression of a network of cycle regulators. Many of these regulators, identified in this and in previous work^{5,6}, are involved in both the cell cycle and the multiciliation cycle, but with different effects. For example, cyclin D1–CDK4/6 is expressed in multiciliated cell precursors and promotes progression of these precursors from a G1/G0-like to an S-like phase to initiate the earliest steps of multiciliated cell differentiation. CDK2 then initiates centriole synthesis during the G1-like to S-like phase transition⁶. From the end of the S-like phase through the G2/M-like phase, the mitotic oscillator CDK1–APC/C regulates centriole growth and disengagement⁵. CDK2 then initiates ciliogenesis as multiciliated cells move into a final G1/G0-like phase, characterized by re-expression of *Cdk4* and *Cdk6*.

This shared use of components raises the question of how the multiciliation cycle redeploys canonical cell cycle regulators while bypassing key steps of the cell cycle such as DNA replication and cell division. The levels of several cell cycle regulators, including *E2f7*, differ between differentiating multiciliated cells and proliferating cells. Investigating the role of *E2f7* in the multiciliation cycle revealed two important functions. First, *E2f7* prevents expression of DNA replication genes in the S-like phase and blocks aberrant DNA synthesis in differentiating multiciliated cells. As *E2f7* is elevated in the S-like phase of the multiciliation cycle to prevent DNA synthesis, CDK1 activity is dampened during the G2/M-like phase of the multiciliation cycle to prevent cytokinesis⁵. The multiciliation cycle uses non-canonical cyclins, such as cyclin A1 and cyclin O, likely to modulate CDK activity during the differentiation^{6,33}.

Still other cell cycle regulators and related proteins may participate in the multiciliation cycle. For example, *Cdkn1a*, which encodes the CDK inhibitor p21^{CIP1}, is upregulated during the S-like and G2/M-like phases of the multiciliation cycle (Fig. 3a), which raises the possibility that it

may restrict CDK1 activity to prevent cell division. *Cdc20b* and *Fbxo43* (also known as *Emi2*) encode cell cycle-related proteins required for centriole disengagement during multiciliated cell differentiation^{41,42}. Thus, numerous cell cycle regulators may be repurposed by the multiciliation cycle to coordinate the construction of a multiciliated cell.

The second function of E2F7 in the multiciliation cycle is to terminate the S-like gene expression program. Without E2F7, S-like phase expression extends into the G2/M-like phase, hallmarks of the G2/M-like phase (such as CCP110 removal and deuterosome disassembly) are delayed, and later events (such as distal appendage formation and ciliogenesis) are disrupted. Consequently, E2F7 was required for multiciliation in the lung, oviduct and brain. As these three tissues are endodermal, mesodermal and ectodermal derivatives, respectively, the multiciliation cycle is likely to be a general regulator of multiciliated cell differentiation.

E2F family members are implicated in two other cell cycle variants, the endocycle and endomitosis^{2,43–46}. Therefore, differential regulation of E2F transcription factors may be a common mechanism by which the canonical cell cycle is repurposed in non-mitotic cells. The endocycle blocks cell division and centriole duplication, whereas the multiciliation cycle omits cell division and chromosome duplication. It will be of interest to assess whether alternative cell cycles coordinate the differentiation of other post-mitotic cell types.

Online content

Any methods, additional references, Nature Portfolio reporting summaries, source data, extended data, supplementary information, acknowledgements, peer review information; details of author contributions and competing interests; and statements of data and code availability are available at <https://doi.org/10.1038/s41586-024-07476-z>.

- Morgan, D. O. *The Cell Cycle: Principles of Control* (New Science Press, 2007).
- Orr-Weaver, T. L. When bigger is better: the role of polyploidy in organogenesis. *Trends Genet.* **31**, 307–315 (2015).
- Choksi, S. P., Lauter, G., Swoboda, P. & Roy, S. Switching on cilia: transcriptional networks regulating ciliogenesis. *Development* **141**, 1427–1441 (2014).
- Spassky, N. & Meunier, A. The development and functions of multiciliated epithelia. *Nat. Rev. Mol. Cell Biol.* **18**, 423–436 (2017).
- Al Jord, A. et al. Calibrated mitotic oscillator drives motile ciliogenesis. *Science* **358**, 803–806 (2017).
- Vladar, E. K. et al. Cyclin-dependent kinase control of motile ciliogenesis. *eLife* **7**, e36375 (2018).
- Walentek, P. Signaling control of mucociliary epithelia: stem cells, cell fates, and the plasticity of cell identity in development and disease. *Cells Tissues Organs* **211**, 736–753 (2022).
- Mahjoub, M. R., Nanjundappa, R. & Harvey, M. N. Development of a multiciliated cell. *Curr. Opin. Cell Biol.* **77**, 102105 (2022).
- Tan, F. E. et al. Myb promotes centriole amplification and later steps of the multiciliogenesis program. *Development* **140**, 4277–4286 (2013).
- Vladar, E. K. & Stearns, T. Molecular characterization of centriole assembly in ciliated epithelial cells. *J. Cell Biol.* **178**, 31–42 (2007).
- Byrnes, L. E., Deleon, R., Reiter, J. F. & Choksi, S. P. Opposing transcription factors MYCL and HEY1 mediate the Notch-dependent airway stem cell fate decision. Preprint at bioRxiv <https://doi.org/10.1101/2022.10.05.511009> (2022).
- Vladar, E. K. & Brody, S. L. in *Methods in Enzymology* Vol. 525 (ed. Marshall, W. F.) 285–309 (Academic Press, 2013).
- Pan, J.-H. et al. Myb permits multilineage airway epithelial cell differentiation. *Stem Cells* **32**, 3245–3256 (2014).
- Lewis, M. & Stracker, T. H. Transcriptional regulation of multiciliated cell differentiation. *Semin. Cell Dev. Biol.* **110**, 51–60 (2021).
- Gomes Pereira, S., Dias Louro, M. A. & Bettencourt-Dias, M. Biophysical and quantitative principles of centrosome biogenesis and structure. *Annu. Rev. Cell Dev. Biol.* **37**, 43–63 (2021).
- Zhao, H. et al. The Cep63 parologue Deup1 enables massive de novo centriole biogenesis for vertebrate multiciliogenesis. *Nat. Cell Biol.* **15**, 1434–1444 (2013).
- Klos Dehring, D. A. et al. Deuterosome-mediated centriole biogenesis. *Dev. Cell* **27**, 103–112 (2013).
- Breslow, D. K. & Holland, A. J. Mechanism and regulation of centriole and cilium biogenesis. *Annu. Rev. Biochem.* **88**, 691–724 (2019).
- Gönczy, P. Centrosomes and cancer: revisiting a long-standing relationship. *Nat. Rev. Cancer* **15**, 639–652 (2015).
- García, S. R. et al. Novel dynamics of human mucociliary differentiation revealed by single-cell RNA sequencing of nasal epithelial cultures. *Development* **146**, dev177428 (2019).
- Ma, L., Quigley, I., Omran, H. & Kintner, C. Multicilin drives centriole biogenesis via E2f proteins. *Genes Dev.* **28**, 1461–1471 (2014).
- Kim, S., Ma, L., Shokhirev, M. N., Quigley, I. & Kintner, C. Multicilin and activated E2f4 induce multiciliated cell differentiation in primary fibroblasts. *Sci. Rep.* **8**, 12369 (2018).
- Plasschaert, L. W. et al. A single-cell atlas of the airway epithelium reveals the CFTR-rich pulmonary ionocyte. *Nature* **560**, 377–381 (2018).
- Montoro, D. T. et al. A revised airway epithelial hierarchy includes CFTR-expressing ionocytes. *Nature* **560**, 319–324 (2018).
- Zheng, S. C. et al. Universal prediction of cell-cycle position using transfer learning. *Genome Biol.* **23**, 41 (2022).
- Grant, G. D., Kedziora, K. M., Limas, J. C., Cook, J. G. & Purvis, J. E. Accurate delineation of cell cycle phase transitions in living cells with PIP-FUCCI. *Cell Cycle* **17**, 2496–2516 (2018).
- Choksi, S. P., Babu, D., Lau, D., Yu, X. & Roy, S. Systematic discovery of novel ciliary genes through functional genomics in the zebrafish. *Development* **141**, 3410–3419 (2014).
- Rubin, S. M., Sage, J. & Skotheim, J. M. Integrating old and new paradigms of G1/S control. *Mol. Cell* **80**, 183–192 (2020).
- Matsushime, H., Roussel, M. F., Ashmun, R. A. & Sherr, C. J. Colony-stimulating factor 1 regulates novel cyclins during the G1 phase of the cell cycle. *Cell* **65**, 701–713 (1991).
- Xiong, Y., Connolly, T., Futcher, B. & Beach, D. Human D-type cyclin. *Cell* **65**, 691–699 (1991).
- Fassl, A., Geng, Y. & Sicinski, P. CDK4 and CDK6 kinases: from basic science to cancer therapy. *Science* **375**, eabc1495 (2022).
- Basant, A. & Glotzer, M. Spatiotemporal regulation of RhoA during cytokinesis. *Curr. Biol.* **28**, R570–R580 (2018).
- Funk, M. C. et al. Cyclin O (Ccno) functions during deuterosome-mediated centriole amplification of multiciliated cells. *EMBO J.* **34**, 1078–1089 (2015).
- Westendorp, B. et al. E2F7 represses a network of oscillating cell cycle genes to control S-phase progression. *Nucleic Acids Res.* **40**, 3511–3523 (2012).
- Li, J. et al. Synergistic function of E2F7 and E2F8 is essential for cell survival and embryonic development. *Dev. Cell* **14**, 62–75 (2008).
- Skene, P. J. & Henikoff, S. An efficient targeted nuclease strategy for high-resolution mapping of DNA binding sites. *eLife* **6**, e21856 (2017).
- Fischer, M., Grossmann, P., Padi, M. & DeCaprio, J. A. Integration of TP53, DREAM, MMB-FOXM1 and RB-E2F target gene analyses identifies cell cycle gene regulatory networks. *Nucleic Acids Res.* **44**, 6070–6086 (2016).
- Kumar, V. et al. The regulatory roles of motile cilia in CSF circulation and hydrocephalus. *Fluids Barriers CNS* **18**, 31 (2021).
- Spektor, A., Tsang, W. Y., Khoo, D. & Dynlach, B. D. Cep97 and CP110 suppress a cilium assembly program. *Cell* **130**, 678–690 (2007).
- Graser, S. et al. Cep164, a novel centriole appendage protein required for primary cilium formation. *J. Cell Biol.* **179**, 321–330 (2007).
- Kim, S., Chien, Y.-H., Ryan, A. & Kintner, C. Emi2 enables centriole amplification during multiciliated cell differentiation. *Sci. Adv.* **8**, eabm7538 (2022).
- Revinski, D. R. et al. CDC20B is required for deuterosome-mediated centriole production in multiciliated cells. *Nat. Commun.* **9**, 4668 (2018).
- Chen, H.-Z. et al. Canonical and atypical E2Fs regulate the mammalian endocycle. *Nat. Cell Biol.* **14**, 1192–1202 (2012).
- Lammens, T., Li, J., Leone, G. & De Leyder, L. Atypical E2Fs: new players in the E2F transcription factor family. *Trends Cell Biol.* **19**, 111–118 (2009).
- Peterson, N. G. & Fox, D. T. Communal living: the role of polyploidy and syncytia in tissue biology. *Chromosome Res.* **29**, 245–260 (2021).
- Edgar, B. A., Zielke, N. & Gutierrez, C. Endocycles: a recurrent evolutionary innovation for post-mitotic cell growth. *Nat. Rev. Mol. Cell Biol.* **15**, 197–210 (2014).

Publisher's note Springer Nature remains neutral with regard to jurisdictional claims in published maps and institutional affiliations.

Springer Nature or its licensor (e.g. a society or other partner) holds exclusive rights to this article under a publishing agreement with the author(s) or other rightsholder(s); author self-archiving of the accepted manuscript version of this article is solely governed by the terms of such publishing agreement and applicable law.

© The Author(s), under exclusive licence to Springer Nature Limited 2024

Methods

Mouse husbandry

Mice were housed under standard pathogen-free conditions at the University of California, San Francisco (UCSF) animal care facility in the Cardiovascular Research Institute under a 12 h light–12 h dark cycle, 30–70% humidity and a temperature of 20–26 °C. All animal protocols and procedures were approved by the Institutional Animal Care and Use Committee of UCSF. Wild-type mice used in these studies were of the strain C57BL/6J, unless otherwise noted, and obtained from Jackson Laboratory (JAX stock 000664). All mice were 6–14 weeks of age at the time of experimentation. All experimental groups were randomized and consisted of mice of both sexes, with an equal number of male and female mice per experiment when possible.

Culturing of mTECs

mTECs were purified and cultured as previously described⁴⁷. Adult mice were anaesthetized with isoflurane. Trachea were removed and placed into 3 mg ml⁻¹ Pronase (Sigma-Aldrich, 10165921001) in Ham's F-12 medium with 100 U ml⁻¹ penicillin and 100 mg ml⁻¹ streptomycin overnight at 4 °C. Trachea were then agitated and cells were plated on Primaria plates (Corning, 087724A) in mTEC basic medium (DMEM/F-12 with 15 mM HEPES, 4 mM L-glutamine, 3.6 mM NaHCO₃, 100 U ml⁻¹ penicillin and 100 mg ml⁻¹ streptomycin) with 10% FBS for 4 h at 37 °C. Airway epithelial cells were collected in mTEC Plus medium (mTEC basic with 10 µg ml⁻¹ insulin (Sigma-Aldrich, I1882), 5 µg ml⁻¹ transferrin (Sigma-Aldrich, T1147), 0.1 µg ml⁻¹ cholera toxin (Sigma-Aldrich, C8052), 25 ng ml⁻¹ epidermal growth factor (Corning, CB40001), 30 µg ml⁻¹ bovine pituitary extract (Sigma-Aldrich, P1476), 5% FBS and 50 nM retinoic acid (Sigma-Aldrich, R2625) and 10 µM ROCK inhibitor (Y-27632, Sigma-Aldrich, Y0503)).

Cells were seeded at a density of 33,000 cells per well on 6.5 mm Transwells (Corning, 3470) coated with 50 µg ml⁻¹ rat tail collagen (type I, Corning, CB354249). Cells were allowed to proliferate for 5 days before initiating differentiation by starting an air–liquid interface culture. The basal chamber contained mTEC basic medium with 2% Nu-Serum (Corning, 355100) and 50 nM retinoic acid, whereas the apical chamber was left empty. Every 2 days, the apical surface was rinsed twice with PBS and the basal medium was changed to fresh mTEC basic medium with 2% Nu-Serum and 50 nM retinoic acid.

scRNA-seq of mTECs

To generate single-cell suspensions of mTECs for scRNA-seq, mTECs were cultured and differentiated as described above. For the differentiation time course, mTECs generated from C57BL/6J adult mice were collected after culture for 1, 3, 9 and 36 days by the air–liquid interface method. For scRNA-seq of mTECs treated with DMSO or ribociclib, ribociclib was added at a final concentration of 10 µM in mTEC basic medium with 2% Nu-Serum and 50 nM retinoic acid at 1 day after air–liquid interface culture and dissociated on day 3 of air–liquid interface culture. For scRNA-seq of mTECs lacking E2F7, mTECs were derived from *E2f7*^{-/-} adult mice or *E2f7*^{+/+} control littermates and dissociated on day 7 of air–liquid interface culture.

Collection consisted of washing mTECs with PBS three times apically and basally, incubating in apical and basal 0.05% trypsin–EDTA in cell dissociation buffer (Gibco, 13151014) for 15 min at 37 °C. Cells were gently triturated and trypsin was inactivated by adding mTEC basic medium with 2% Nu-Serum. An additional collection of cells was performed by adding 0.05% trypsin–EDTA in cell dissociation buffer apically for 5 min at 37 °C. Both collections were combined, washed, centrifuged and resuspended in 0.04% BSA in PBS at a density of 1,000 cells per µl.

For the transcriptional time course, 10,000 mTECs at day 1 of air–liquid interface culture were loaded onto each of 4 separate wells. On day 3, 9 or 36, 25,000 mTECs were loaded onto separate wells of a 10x Chromium Controller using a Chromium Single Cell 3' Reagent kit

(10x Genomics, v.3, PN-1000075). For the analysis of mTECs treated with DMSO or ribociclib, 16,500 cells from each of 3 independent replicate mTECs were loaded onto 6 separate wells of the 10x Chromium Controller. For the analysis of E2F7 function, 16,000 cells from each of 2 independent replicates of *E2f7*^{+/+} and *E2f7*^{-/-} mTECs were loaded onto 4 separate wells of the 10x Chromium Controller. Manufacturer's instructions were followed for gel beads-in-emulsion generation, cDNA production and library construction. Libraries were sequenced with an Illumina NovaSeq and NextSeq. CellRanger 3.0 (time course dataset), 7.1 (DMSO and ribociclib dataset) or 7.0 (*E2f7* dataset) was used with default settings to demultiplex, align reads to the mouse genome (modified mm10 genome 3.0.0, <https://www.10xgenomics.com/support/software/cell-ranger/downloads/cr-ref-build-steps#mouse-ref-3-0-mm10-vdj>) and to count unique molecular identifiers. Cellranger aggr was used to aggregate technical replicates of mTECs on day 1 of air–liquid interface culture. Doublets were identified and removed from individual datasets with Scrublet (v.0.2.1)⁴⁸ for the time course and *E2f7* datasets or DoubletFinder (v.2.0)⁴⁹ for the DMSO and ribociclib dataset with an assumed doublet rate based on loading concentrations. SoupX (v.1.5.0)⁵⁰ was used to remove ambient background RNA from droplets of wild-type time course and DMSO and ribociclib datasets. Seurat (v.4)⁵¹ was used for downstream analysis of individual datasets, including filtering, dimension reduction, clustering, UMAP and differential gene expression analysis.

Individual scRNA-seq datasets were merged using Seurat integration to correct for batch effects. One replicate from each of days 1, 3, 9 and 36 of air–liquid interface culture was integrated to produce the time course dataset. Three replicates of DMSO-treated and ribociclib-treated mTECs were integrated to produce the DMSO and ribociclib dataset. Two replicates of *E2f7*^{+/+} and *E2f7*^{-/-} mTECs were integrated to produce the *E2f7* dataset. Dimension reduction and clustering using the Louvain algorithm were performed in Seurat. Basal-stem-cell-focused or multiciliated-cell-focused datasets were subclustered and reanalysed as described above. In both the time course and *E2f7* datasets, a subcluster of mature multiciliated cells that shared gene expression with other cell types was removed from further analysis. Trajectory inference was performed with Monocle3 (v.1.2)⁵², using as.Celldata to import the dataset from Seurat. Marker genes were identified using FindAllMarkers. Potential differences in cell type proportions were tested with Speckle (v.0.99.7)⁵³ for the *E2f7* dataset and cell cycle phase proportions in the DMSO and ribociclib dataset and edgeR (v.3.40.2)⁵⁴ glmQLFit for cell type proportions in the DMSO and ribociclib dataset.

Genes annotated with the 'cell cycle' GO term (GO:0007049) and genes from previously generated S and G2M phase gene lists⁵⁵ were tested for enrichment in basal stem cells and multiciliated cells with FindAllMarkers. Cell cycle phase scores were predicted with Tricycle (v.1.6.0)²⁵, using the default reference dataset. S and G2/M scores were calculated with UCell (v.2.2.0)⁵⁶, using previously generated S and G2/M phase gene lists⁵⁵. Analysis of differential gene expression between *E2f7*^{+/+} and *E2f7*^{-/-} clusters and DMSO and ribociclib clusters was performed using DESeq2 (v.1.38.3)⁵⁷. Smooth lines depicting gene expression across pseudotime were generated using ggplot2 (v.3.4.2)⁵⁸ geom_smooth.

To investigate cytoskeletal factors that may contribute to phenotypes observed in *E2f7*^{-/-} multiciliated cells, 521 genes encoding annotated cytoskeletal regulators (GO biological process terms containing 'cytoskeleton') were intersected with differentially expressed genes between *E2f7*^{-/-} and *E2f7*^{+/+} multiciliated cells (Extended Data Fig. 8a and Supplementary Table 7).

Lentiviral production and transduction of mTECs

The pLenti-PGK-Neo-PIP-FUCCI²⁶ plasmid was obtained from Addgene (118616). For expression of NLS–GFP, cyclin D1–GFP or E2F7–GFP, the coding sequence of NLS was synthesized and mouse *Ccnd1* (ENSMUST00000093962.5) or *E2f7* were PCR-amplified

Article

(ENSMUST00000073781.12) and cloned with a sequence encoding a carboxy-terminal eGFP into pLKO.3G (Addgene, 14748) with the sgRNA expression cassette removed. Lentivirus was generated by transfecting 7.5 µg of each plasmid with 1.5 µg of pCMV-VSV-G (Addgene, 8454) and 6 µg of psPAX2 (Addgene, 12260) into a 10 cm plate of Lenti-X 293T cells (HEK 293T, Takara) at 70–80% confluence using Fugene 6 transfection reagent (Promega, E2691). Medium containing lentiviral particles were collected at 1, 2 and 3 days after transfection and concentrated by centrifugation at 25,000 r.p.m. for 1.5 h at 4 °C, and the pellet was resuspended in 300 µl PBS.

For lentiviral transduction of mTECs, cells were isolated from mouse trachea as described above. Cells were plated in 6.5 mm Transwells and transduced with 1–20 µl of lentivirus in mTEC Plus medium supplemented with 50 nM retinoic acid and 10 µM ROCK inhibitor as previously described⁵⁹. Basal medium was changed 1 day after transduction and apical medium was changed 2 days after transduction. Medium in both chambers was changed at 3 days after transduction, and mTECs were differentiated by air–liquid interface culture, as described above.

Immunofluorescence of mTECs

For paraformaldehyde (PFA) fixation, cells on Transwells were washed 3 times in PBS and fixed in 4% PFA in PBS for 10 min at room temperature. Cells were rinsed three times with PBS and Transwell membranes were removed using a scalpel and then cut into smaller pieces. An individual piece of membrane was placed on a slide inside a hydrophobic boundary for staining. Cells were blocked for 1 h at room temperature in PBT (1% BSA, 0.5% Triton X-100 and 0.02% sodium azide in PBS) supplemented with 10% normal donkey serum.

For the Triton–PFA fixation, cells on Transwells were washed as above, then 0.5% Triton X-100 in PBS was added to apical and basal chambers. After a 3 min incubation, Triton X-100 was removed and cells were fixed in 4% PFA in PBS for 10 min at room temperature. Cells were rinsed and cut as above. Once on the slide, cells were incubated in 0.5% Triton-X-100 in PBS for 15 min at room temperature. After 3 washes in PBS for 5 min each, cells were blocked 1 h at room temperature in PBT as above.

For both PFA-fixed and Triton–PFA-fixed cells, cells were then incubated in primary antibody diluted in PBT for 1 h at room temperature. After 5 PBS washes of 5 min each, secondary antibodies diluted in PBT were added for 1 h at room temperature. Secondary antibodies were washed off as for the primary antibody. Hoechst, phalloidin or βIV-tubulin were added to stain nuclei, actin or cilia, respectively, either during the secondary incubation or as a tertiary stain. Tertiary stains were removed with 5 PBS washes of 5 min each.

Cells were then mounted in Prolong Diamond Antifade (Molecular Probes, P36970) medium. Primary and secondary antibodies, tertiary stains, dilutions and fixation conditions are provided in Supplementary Table 10. For all mTEC immunofluorescence experiments, biological replicates refer to independently derived mTEC populations.

EdU labelling and detection

For EdU labelling, 10 µM EdU or DMSO was added to basal medium of mTECs at 1 day after initiation of air–liquid interface culture. Medium with fresh EdU or DMSO was changed every other day until 5 days of air–liquid interface culture, at which point cells on Transwells were washed 3 times in PBS and fixed in 4% PFA in PBS for 15 min at room temperature. PFA was washed off cells with three rinses with PBS and Transwell membranes were removed, cut and placed on a slide inside a hydrophobic boundary for staining. Cells were permeabilized with a 20-min incubation in 0.5% Triton X-100 in PBS at room temperature, followed by a 30-min incubation in Click-iT EdU reaction buffer using Azide-AlexaFluor-488 (Thermo Fisher, C10337). Cells were rinsed once with PBS, then blocked for 1 h at room temperature in PBT (1% BSA, 0.5% Triton X-100 and 0.02% sodium azide in PBS) supplemented with 10%

normal donkey serum. The remaining immunofluorescence detection protocol proceeded as described above.

PIP–FUCCI cell cycle analysis

For mTECs transduced with PIP–FUCCI lentivirus, cells were fixed with PFA after 3 days of air–liquid interface culture and were stained with antibodies to detect centrioles (CEP43) or cilia (βIV-tubulin) as described above. For nuclear PIP–FUCCI imaging, images were collected at a zoom of ×1 to prevent photobleaching. To stage multiciliated cell differentiation, the same cells were then imaged at ×3 zoom and with AIRYscan superresolution imaging. The mean nuclear fluorescence of the PIP–FUCCI reporters was assessed in ImageJ (v.1.53c) by manually drawing a region of interest around the nucleus of multiciliated cells and measuring mean fluorescence of both mVenus and mCherry. Multiciliated cells were independently staged based on the superresolution imaging of CEP43 and αTUB^{Ac}, as described (Extended Data Fig. 1). Multiciliated cell staging was then matched with the corresponding nuclear PIP–FUCCI fluorescence levels. Three independently derived mTEC populations were transduced separately for the 3 biological replicates of PIP–FUCCI scoring, and at least 44 multiciliated cells were quantified per biological replicate.

CDK4/6 modulation in differentiating mTECs

To evaluate the effects of CDK4/6 activity inhibition in mTECs, DMSO (vehicle control), palbociclib or ribociclib was added to a final concentration of 10 µM in mTEC basic medium with 2% Nu-Serum and 50 nM retinoic acid and added to the basal chamber of mTECs during differentiation. Medium with fresh DMSO, palbociclib or ribociclib was changed every other day until the day of collection. DMSO, palbociclib or ribociclib treatment was started at different times during differentiation in an experiment-specific manner. For immunofluorescence experiments, drugs were delivered from days 1–5 of differentiation by air–liquid interface culture (Fig. 2b–e and Extended Data Fig. 5c). For generating the DMSO and ribociclib scRNA-seq dataset, drugs were delivered from days 1–3 of differentiation by air–liquid interface culture (Fig. 2f–k, and Extended Data Fig. 5d–h). For evaluation of delivery timing, drugs were added at days 0–5 or 2–5 of differentiation by air–liquid interface culture, as indicated (Extended Data Fig. 5a–c).

To evaluate the effects of CDK4/6 activity overactivation in mTECs, lentivirus encoding NLS–GFP (control) or cyclin D1–GFP was delivered as described above. Cells were fixed for immunofluorescence at 5 days of differentiation by air–liquid interface culture.

CRISPR–Cas9 mutant mouse generation

To generate *E2f7*^{-/-} mice, 180 pmol of sgRNA targeting the exon encoding the DNA-binding domain of E2F7 was mixed with 2.5 µg of TrueCut Cas9 v2 (Thermo Fisher, A36499) and incubated at room temperature for 15 min to allow for the formation of ribonucleoprotein (RNP) complexes. RNP complexes were brought up to 100 µl with Tris–EDTA and filtered twice through a 0.1 mm PVDF filter (Millipore, UFC30VV25). RNPs were microinjected into zygotes from primed and mated CD-1 female mice and transferred into recipient females. Pups were screened by PCR and sequencing, and founder lines were crossed to C57BL/6J mice to generate heterozygous mutant lines.

Whole-mount brain immunofluorescence

Brains were dissected and lateral walls exposed, washed once with PBS, then fixed for 10 min in ice cold methanol. Tissue was washed once with PBS for 5 min and then fixed overnight in 4% PFA at 4 °C overnight. Tissue was washed 3 times for 10 min in PBS, then blocked for 1 h in 10% normal donkey serum with 0.03% Triton X-100 in PBS at room temperature. Primary and secondary antibodies were diluted in 10% normal donkey serum with 0.03% Triton X-100 in PBS and incubated at 4 °C overnight, with 3 times 10 min washes in PBS containing 0.03%

Triton X-100 after each incubation. Tissue was then mounted and imaged in Prolong Diamond Antifade medium.

Tissue cryosectioning and immunofluorescence

Tissues were dissected from mice and fixed overnight in 4% PFA, then were washed 3 times in PBS and placed into 30% sucrose until tissues descended. Tissues were embedded in OCT and sections taken on a Leica CM1900 cryostat at 10 µm thickness. Sections were collected on glass slides and allowed to dry for at least 1 h before staining. For staining, sections were washed 3 times in PBST (0.1% Tween-20 diluted in PBS). Next, citrate antigen retrieval was performed 3 times with boiling 0.1 M citrate buffer with 0.1% Tween-20 at pH 6.0. Tissues were then washed once with PBST and blocked for 1 h in 10% normal donkey serum in PBST at room temperature. Primary antibodies were diluted in PBST + 10% normal donkey serum and placed on slides for 1.5 h at room temperature or overnight at 4 °C. Slides were washed 3 times in PBST and secondary antibody was added for 1 h at room temperature. Slides were washed 5 times for 5–10 min each in PBST and mounted with Prolong Diamond Antifade medium.

Histological staining and quantitation of brain phenotypes

Slides were washed 3 times in PBS for 5 min each, then washed in ddH₂O twice for 3 min each. Slides were placed in haematoxylin for 3 min then washed for 1 min in running tap water. Slides were then placed in clarifier for 1 min, washed for 30 s in ddH₂O and placed into Bluing Reagent for 1 min. Slides were then washed for 30 s in ddH₂O. Slides were then placed in 80% ethanol for 1 min and stained in eosin Y for 3 min. The slides were progressively dehydrated in ethanol from 95 to 100% for 2 washes of 2 min each, then dehydrated in xylene twice for 3 min each and mounted using Cytoseal (Thermo Fisher, 23-244257). Slides were imaged on a Leica Widefield DMI8 microscope equipped with a Leica DFC9000 GTC camera.

To quantitate ventricle size, a ratio of the ventricular area to the whole brain area was calculated using the line segment tool in ImageJ (v.1.53c). Three coronal sections from each animal were averaged to calculate ventricular area of three animals per genotype.

CUT&RUN

CUT&RUN was performed as previously described^{36,60}, with protocol and buffers detailed in protocol 2 (ref. 61). In brief, E2F7-GFP-transduced or NLS-GFP-transduced mTECs were grown on 24 mm Transwells (Corning, 3450) for 3 days in air–liquid interface culture and were dissociated in 0.05% trypsin–EDTA in cell dissociation buffer for 15 min at 37 °C. Cells were collected in mTEC basic medium with 2% Nu-Serum, washed twice in 5 ml of CUT&RUN wash buffer and resuspended in CUT&RUN wash buffer. One million cells of each sample were brought up to a volume of 1 ml with CUT&RUN wash buffer. Cells were incubated with 10 µl activated wheat germ agglutinin beads (Bangs Laboratories, BP530) at room temperature for 10 min with gentle rocking. Cells were incubated overnight with rabbit anti-GFP antibody (Abcam, ab290) diluted 1:100 in 0.05% digitonin in CUT&RUN wash buffer. Following 2 washes in CUT&RUN wash buffer, samples were incubated for 1 h at room temperature in guinea pig anti-Rabbit IgG (Rockland, 611-201-122) diluted 1:100 in 0.05% digitonin in CUT&RUN wash buffer. Samples were incubated with Protein A/G–MNase fusion protein (Addgene, 123461) at 700 ng ml⁻¹ for 1 h at 4 °C. Following 2 washes in 0.05% digitonin in CUT&RUN wash buffer and one wash in CUT&RUN low-salt rinse buffer, samples were digested for 10 min at 0 °C in cold CUT&RUN incubation buffer. DNA fragments were released by incubation at 37 °C for 30 min and then collected in the aqueous phase of a phenol–chloroform extraction. Library preparation was performed using a Next Ultra II DNA Library Prep kit for Illumina (NEB, E7645S) using 25 µl of CUT&RUN DNA as input, as previously detailed⁶². Adaptors were diluted 1:15 in adaptor dilution buffer. High

sensitivity D5000 ScreenTape reagents (Agilent, 5067-5593) and the Tapestation 4200 (Agilent) were used to assess library quality and pool libraries for sequencing. Sequencing was done using a NextSeq 500 (Illumina).

CUT&RUN analysis was performed using previously described scripts^{63,64}. In brief, FASTQs were trimmed using trimomatic (v.0.39)⁶⁵ with a second trimming step to remove remaining read-through adaptors. Reads were aligned with bowtie2 (v.2.4.2)⁶⁶ using the parameters --local --very-sensitive-local --no-unal --no-mixed --no-discordant --phred33-I10-X 700. Samples were filtered for reads under 120 bp and duplicates were marked, but not removed, with samtools (v.1.10) and picard (v.2.24.0) MarkDuplicates. MACS2 (v.2.1.2)⁶⁷ was used to call peaks using parameters --keep-dup all -q 0.05 and -c with the corresponding control being the NLS–GFP sample. Final peak list was generated by the intersection of replicate peak lists. ChIPseeker (v.1.34.1)⁶⁸ was used to annotate peaks to the nearest gene.

Quantitative PCR with reverse transcription

Total RNA was extracted from mTECs at 3 days of differentiation by air–liquid interface culture using a RNeasy Plus Mini kit (Qiagen, 74134). Reverse transcription of 300–1,000 ng of RNA was carried out for 1 h at 42 °C using a iSCRIPT cDNA synthesis kit (Bio-Rad, 1708841BUN). Quantitative PCR was performed using a QuantStudio 5 real-time PCR machine running QuantStudio Design & Analysis software (v.1.5.1) (Applied Biosystems) and using PowerUp SYBR green master mix (Applied Biosystems, A25742). A table of primer sequences is provided in Supplementary Table 10. Relative expression was calculated using the ΔΔCT method⁶⁹. An average of three control gene (*Hprt*, *Actb* and *Rplp0*) expression levels was used for internal sample normalization. All quantitative PCR with reverse transcription experiments were carried out on at least three independently derived and treated mTEC cultures.

Image acquisition and analysis

Immunofluorescence images were acquired on a Zeiss 800 laser scanning confocal microscope with Airyscan superresolution capability and equipped with a ×63 oil objective. ZEN microscopy software (v.3.7; Zeiss) was used for image acquisition. All images were processed using ImageJ (v.1.53c) and figures were assembled in Adobe Illustrator.

At least three randomly selected regions of stained membrane were imaged for each biological replicate per each condition, with a minimum of three biological replicates per experiment. At each position, a stack of 10–20 images was collected, spaced 0.5 µm apart in the z axis with no additional zoom. For superresolution imaging, stacks were spaced 0.14 µm apart and collected at ×3 zoom.

Gain and laser power were held constant for each channel for each experiment. Images were processed identically using ImageJ (v.1.53c) to generate maximum projections for figure assembly. Sum projections were created for fluorescence intensity quantification. Significance testing was performed in Prism (v.9.5.1).

Generating CRISPR knockout mTECs

mTECs were isolated as described above and 175,000 cells were seeded on 24 mm collagen-coated Transwells (Corning, 3450) in mTEC Plus Expansion medium (mTEC Plus supplemented with 50 nM retinoic acid, 10 µM ROCK inhibitor, 1 µM A83-01 (Tocris, 2939), 200 nM DMH-1 (Tocris, 4126) and 500 nM CHIR99021 (Tocris, 4423)) based on a previously described recipe⁷⁰. Expansion medium was changed daily for 4 days. Cells were then dissociated using 0.05% trypsin diluted in cell dissociation buffer (Gibco, 13151014) and collected, counted, washed in PBS and resuspended in P3 electroporation buffer (Lonza, V4SP-3096) at a concentration of 20,000 cells per 1 µl.

Guide RNAs targeting *E2f8* or two control nontargeting guides were designed and synthesized (Synthego; sequences in Supplementary

Article

Table 10). RNPs were assembled by incubating 90 pmol TrueCut Cas9 v2 protein (Thermo Fisher, A36499) with 180 pmol of sgRNA at room temperature for 15 min. A total of 400,000 cells in 20 µl of P3 buffer were added to each RNP and electroporated using program 96-EA-104 on an Amaxa 4D-Nucleofector equipped with a 96-well shuttle (Lonza, AAF-1003B/S). After electroporation, cells were collected in mTEC Plus Expansion medium and seeded equally onto five 6.5 mm collagen-coated Transwells. Expansion medium was changed daily until cells reached confluence (3–4 days after electroporation) at which point cells were differentiated similar to standard mTECs as described above.

To evaluate knockout efficiency, gDNA was extracted from a single 6.5 mm Transwell using an AllPrep DNA/RNA Mini kit (Qiagen, 0204). gDNA was amplified using oligonucleotides surrounding the sgRNA binding site. PCR amplicons were purified and Sanger sequenced using the corresponding forward primer. Sequence data were deconvolved and analysed using ICE to determine knockout efficiency (<https://ice.synthego.com/>). A minimum of three independently derived and electroporated mTEC populations per guide RNA were generated for analysis of knockout efficiency and phenotypes.

Transmission electron microscopy of mTECs

mTECs were differentiated for 7 days by air–liquid interface culture and fixed in 4% PFA and 2% glutaraldehyde in 0.1 M sodium cacodylate buffer. Subsequently, cells were washed 3 times with 0.1 M sodium cacodylate buffer, followed by post-fixation with 1% osmium tetroxide. This was followed by 3 washes with ddH₂O and pre-staining with 0.5% uranyl acetate for 1 h, followed by 3 additional washes with ddH₂O. Cells were dehydrated with graded ethanol and inserts were removed from the Transwell and placed on a piece of ACLAR film. Poly/Bed 812 resin (Polysciences, 08792-1) was added directly onto the inserts. A thin resin slide, approximately 2 mm thick, was sectioned from the polymerized resin block near the bottom of the insert using a jeweller's saw blade. The resin slide was sliced into 1 mm blocks using a razor blade and glued onto a supporting resin block, with the surface where the cells had grown positioned sideways. The other sides of the block without cells were further trimmed, and 70 nm sections were sliced using a Leica EM UC7 microtome and diamond knife. TEMs were obtained using a transmission electron microscope (FEI T12) equipped with a CCD camera.

Obtaining biological materials

All biological materials generated in this study are available upon request.

Statistical testing

All statistical testing was performed using Prism (v.9.5.1). Statistical tests used for each experiment are listed in the accompanying figure legend.

Reporting summary

Further information on research design is available in the Nature Portfolio Reporting Summary linked to this article.

Data availability

scRNA-seq and CUT&RUN raw FASTQ files and processed data have been deposited into the Gene Expression Omnibus database under accession GSE228110. scRNA-seq datasets have been deposited in the CellxGene single cell browser (<https://cellxgene.cziscience.com/collections/c26ca66a-63ea-4059-a24e-0e0be0a2a173>). The mouse mm10 reference genome was downloaded for analysis and is available from 10x Genomics (<https://www.10xgenomics.com/support/software/cell-ranger/downloads/cr-ref-build-steps#mouse-ref-3-0-mm10-vdj>). Source data are provided with this paper.

Code availability

Scripts are available at GitHub (https://github.com/lb15/multiciliation_cycle). Scripts and R objects used for analysis are available at Zenodo (<https://doi.org/10.5281/zenodo.10896100>)⁷¹, including CUT&RUN analysis scripts (<https://doi.org/10.5281/zenodo.10896066>)⁷² and Seurat analysis scripts (<https://doi.org/10.5281/zenodo.10896071>)⁷³.

47. You, Y. & Brody, S. L. Culture and differentiation of mouse tracheal epithelial cells. *Methods Mol. Biol.* **945**, 123–143 (2013).
48. Wolock, S. L., Lopez, R. & Klein, A. M. Scrublet: computational identification of cell doublets in single-cell transcriptomic data. *Cell Syst.* **8**, 281–291.e9 (2019).
49. McGinnis, C. S., Murrow, L. M. & Gartner, Z. J. DoubletFinder: doublet detection in single-cell RNA sequencing data using artificial nearest neighbors. *Cell Syst.* **8**, 329–337.e4 (2019).
50. Young, M. D. & Behjati, S. SoupX removes ambient RNA contamination from droplet-based single-cell RNA sequencing data. *Gigascience* **9**, giaa151 (2020).
51. Stuart, T. et al. Comprehensive integration of single-cell data. *Cell* **177**, 1888–1902.e21 (2019).
52. Cao, J. et al. The single-cell transcriptional landscape of mammalian organogenesis. *Nature* **566**, 496–502 (2019).
53. Phipson, B. et al. propeller: testing for differences in cell type proportions in single cell data. *Bioinformatics* **38**, 4720–4726 (2022).
54. Robinson, M. D., McCarthy, D. J. & Smyth, G. K. edgeR: a Bioconductor package for differential expression analysis of digital gene expression data. *Bioinformatics* **26**, 139–140 (2010).
55. Kowalczyk, M. S. et al. Single-cell RNA-seq reveals changes in cell cycle and differentiation programs upon aging of hematopoietic stem cells. *Genome Res.* **25**, 1860–1872 (2015).
56. Andreatta, M. & Carmona, S. J. UCell: robust and scalable single-cell gene signature scoring. *Comput. Struct. Biotechnol. J.* **19**, 3796–3798 (2021).
57. Love, M. I., Huber, W. & Anders, S. Moderated estimation of fold change and dispersion for RNA-seq data with DESeq2. *Genome Biol.* **15**, 550 (2014).
58. Wickham, H., Navarro, D. & Pedersen, T. L. *ggplot2: Elegant Graphics for Data Analysis* 3rd edn <https://ggplot2-book.org/> (Springer, 2024).
59. Horani, A., Nath, A., Wasserman, M. G., Huang, T. & Brody, S. L. Rho-associated protein kinase inhibition enhances airway epithelial basal-cell proliferation and lentivirus transduction. *Am. J. Respir. Cell Mol. Biol.* **49**, 341–347 (2013).
60. Meers, M. P., Bryson, T. D., Henikoff, J. G. & Henikoff, S. Improved CUT&RUN chromatin profiling tools. *eLife* **8**, e46314 (2019).
61. Janssens, D. & Henikoff, S. CUT&RUN: targeted *in situ* genome-wide profiling with high efficiency for low cell numbers. *protocols.io* <https://doi.org/10.17504/protocols.io.zcpf2vn> (2019).
62. Liu, N. Library prep for CUT&RUN with NEBNext® Ultra™ II DNA Library Prep Kit for Illumina® (E7645). *protocols.io* <https://doi.org/10.17504/protocols.io.bagaibse> (2021).
63. Zhu, Q., Liu, N., Orkin, S. H. & Yuan, G.-C. CUT&RUNTools: a flexible pipeline for CUT&RUN processing and footprint analysis. *Genome Biol.* **20**, 192 (2019).
64. Zheng, Y., Ahmad, K. & Henikoff, S. CUT&Tag data processing and analysis tutorial. *protocols.io* <https://doi.org/10.17504/protocols.io.bjk2kkye> (2020).
65. Bolger, A. M., Lohse, M. & Usadel, B. Trimmomatic: a flexible trimmer for Illumina sequence data. *Bioinformatics* **30**, 2114–2120 (2014).
66. Langmead, B. & Salzberg, S. L. Fast gapped-read alignment with Bowtie 2. *Nat. Methods* **9**, 357–359 (2012).
67. Zhang, Y. et al. Model-based analysis of ChIP-seq (MACS). *Genome Biol.* **9**, R137 (2008).
68. Yu, G., Wang, L.-G. & He, Q.-Y. ChIPseeker: an R/Bioconductor package for ChIP peak annotation, comparison and visualization. *Bioinformatics* **31**, 2382–2383 (2015).
69. Livak, K. J. & Schmittgen, T. D. Analysis of relative gene expression data using real-time quantitative PCR and the 2($^{-\Delta\Delta T}$) method. *Methods* **25**, 402–408 (2001).
70. Mou, H. et al. Dual SMAD signaling inhibition enables long-term expansion of diverse epithelial basal cells. *Cell Stem Cell* **19**, 217–231 (2016).
71. lb15_multiciliation_cycle: v1.1.3. Zenodo <https://doi.org/10.5281/zenodo.10896100> (2024).
72. lb15_autoCutandRun: v1.1.1. Zenodo <https://doi.org/10.5281/zenodo.10896066> (2024).
73. lb15_autoSeurat: v1.1.2. Zenodo <https://doi.org/10.5281/zenodo.10896071> (2024).

Acknowledgements We thank D. Erle, K. D. Koh and L. Bonser for advice on developing the CRISPR knockout protocol; E. Yu for mouse husbandry; D.O. Morgan, P.H. O'Farrell, M. Aydogan, P.K. Choksi and members of the Reiter Laboratory for critical discussion; N. Neff, R. Sit and M. Tan from the CZ Biohub Genomics platform for sequencing; and staff at the UCSF Laboratory for Cell Analysis and the UCSF Center for Advanced Cell Technology for use of equipment and the Wynton high performance computing cluster for analysis. L.E.B was supported by Ruth L. Kirschstein National Research Service Awards (5T32HL007731-27 and 1F32HL154611-01). This work was supported by a CIRM Discovery grant (DISC1-10475) to S.P.C. and grants from the NIH (R01AR054396 and R01HD089918) to J.F.R. This research was also supported by the National Cancer Institute, National Institutes of Health, Intramural Research Program, and was funded in whole or in part with federal funds from the National Cancer Institute, National Institutes of Health under contract HHSN26120080001E. The content of this publication does not necessarily reflect the views or policies of the Department of Health and Human Services, nor does mention of trade names, commercial products, or organizations imply endorsement by the US Government.

Author contributions S.P.C. conceptualized the study. S.P.C., L.E.B. and J.F.R. designed experiments. S.P.C. and L.E.B. performed experiments and analysed data. L.E.B. performed bioinformatics analyses. M.J.K. performed phenotypic analyses of mouse mutants. B.W.H.T. and R.D. assisted with experimentation. Q.L. and C.J.W. performed transmission electron microscopy analyses. S.P.C., L.E.B. and J.F.R. wrote the manuscript. S.P.C. and J.F.R. supervised the research. All authors reviewed and edited the manuscript.

Competing interests J.F.R. cofounded startup companies funded by BridgeBio and 459AM.

Additional information

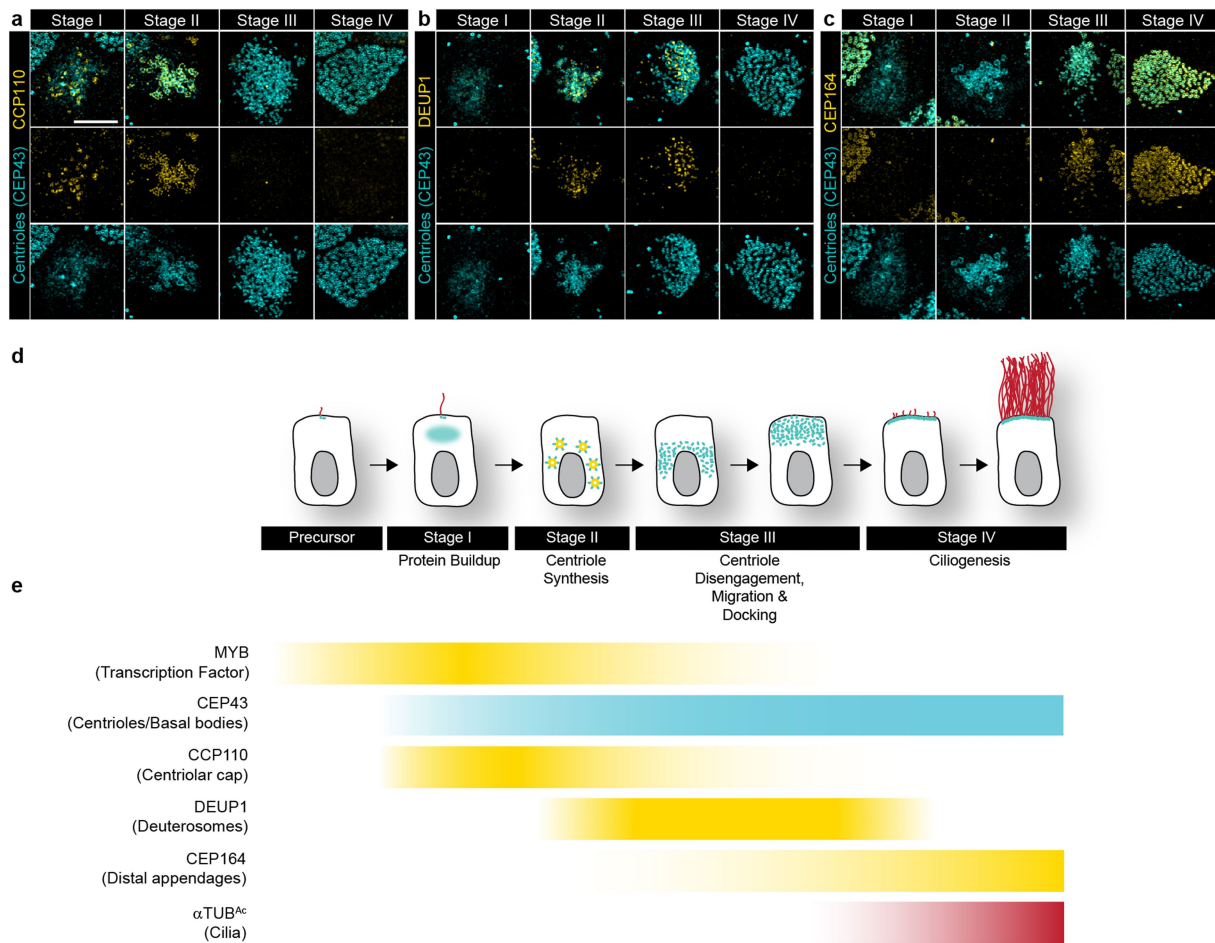
Supplementary information The online version contains supplementary material available at <https://doi.org/10.1038/s41586-024-07476-z>.

Correspondence and requests for materials should be addressed to Semil P. Choksi or Jeremy F. Reiter.

Peer review information *Nature* thanks Piotr Sicinski, Bart Westendorp and the other, anonymous, reviewer(s) for their contribution to the peer review of this work. Peer reviewer reports are available.

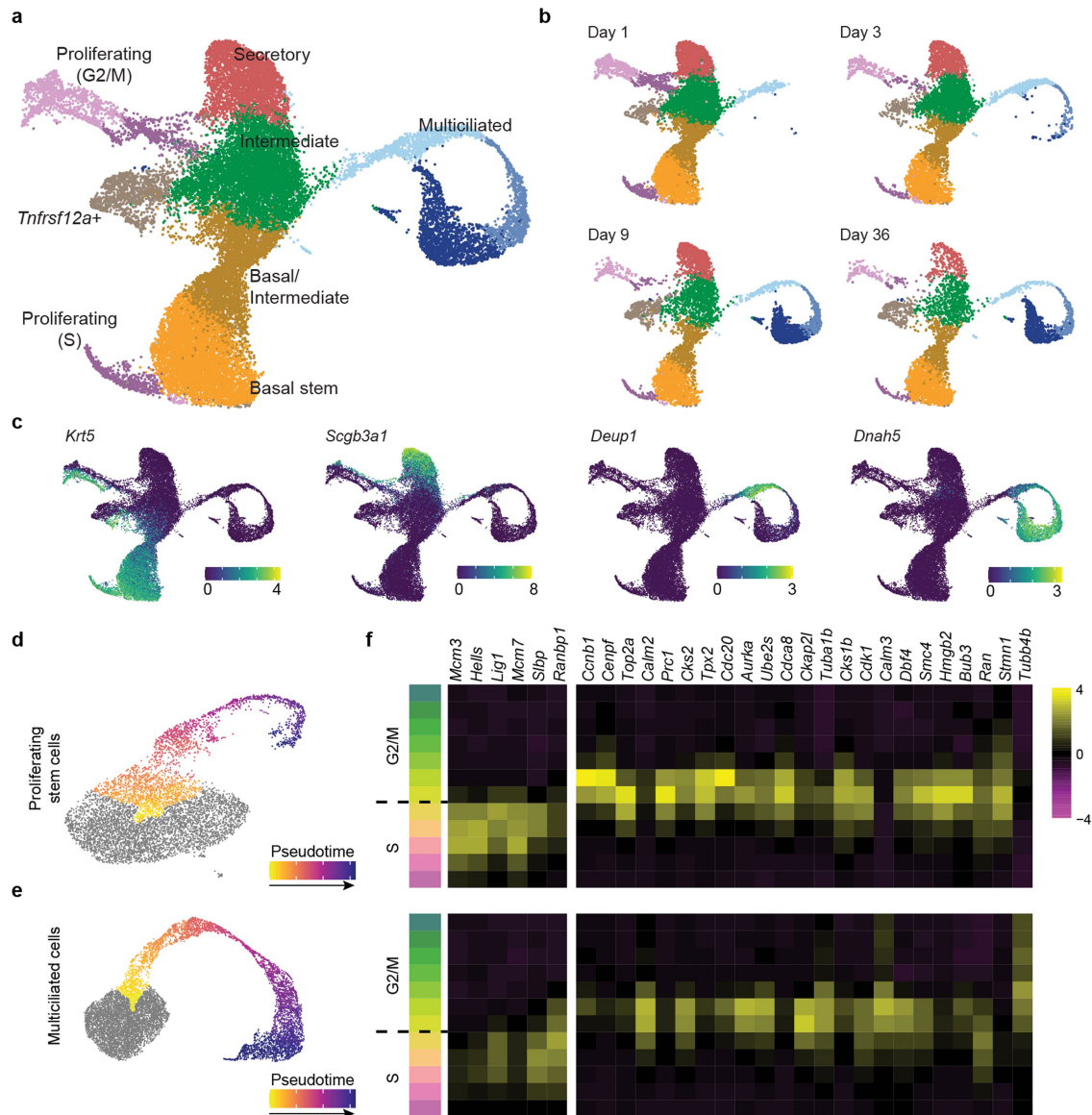
Reprints and permissions information is available at <http://www.nature.com/reprints>.

Article



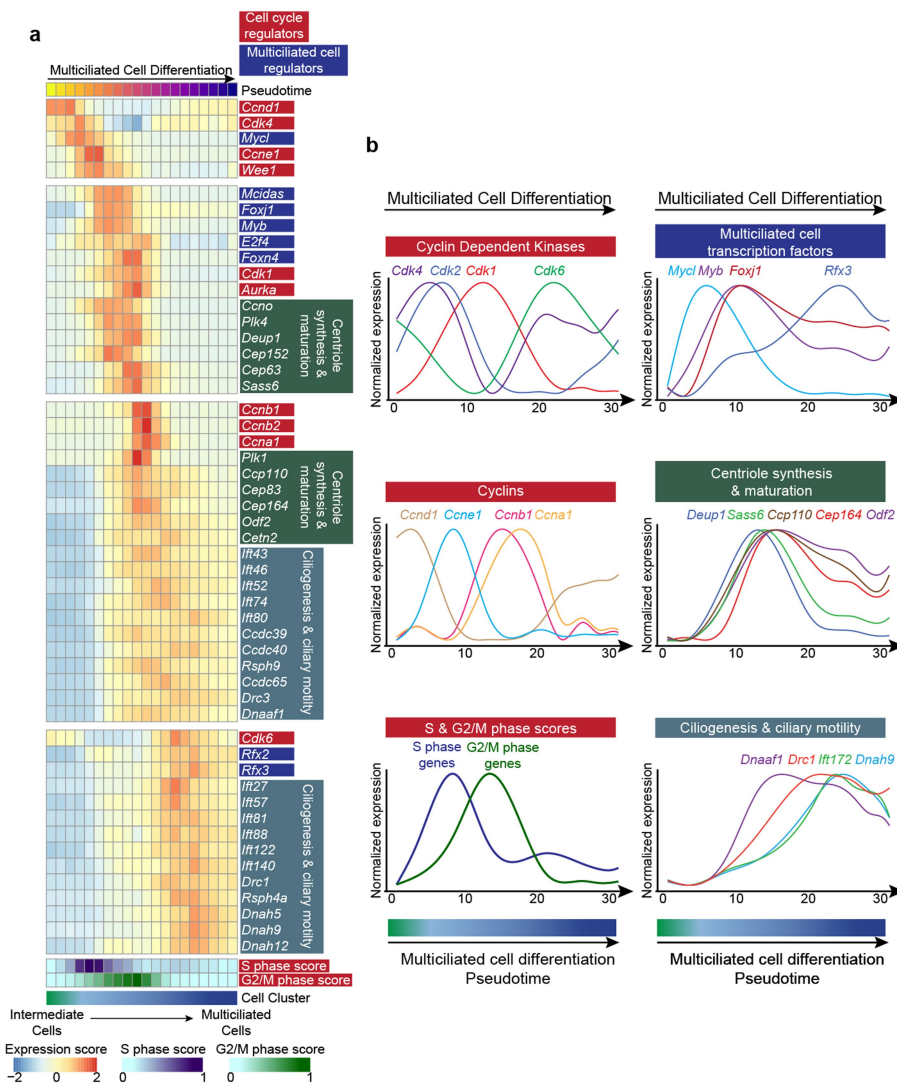
Extended Data Fig. 1 | Multiciliated cells go through sequential stages of differentiation. **a**, Representative immunofluorescence images of wild-type mTECs cultured at air-liquid interface for three days and stained for centrioles (CEP43, cyan) and CCP110 (yellow). Cells at stages I–IV of multiciliated differentiation are depicted. n = 3 biological replicates. Scale bar, 5 μ m. **b**, Representative immunofluorescence images of wild-type mTECs cultured at air-liquid interface for three days and stained for centrioles (CEP43, cyan) and deuterosomes (DEUP1, yellow). n = 3 biological replicates. **c**, Representative immunofluorescence images of wild-type mTECs cultured at air-liquid interface for three days and stained for centrioles (CEP43, cyan) and distal appendages (CEP164, yellow). n = 3 biological replicates. **d**, A schematic of the stages of

multiciliated cell differentiation. Precursors induce the expression of early multiciliated cell transcription factors, such as MYB. Stage I involves the induction of proteins required for centriole biogenesis, such as CEP43 and CCP110. Stage II involves the generation of deuterosomes (marked by DEUP1, depicted here as yellow circles) and the synthesis of centrioles (depicted as blue dots). Stage III involves centriole disengagement, migration, acquisition of distal appendages (marked by CEP164) and docking at the apical membrane. Stage IV involves ciliogenesis. Cilia are in red. **e**, Proteins that are expressed during each stage of multiciliated cell differentiation used in this study are listed, with expression in precursors and during multiciliated cell differentiation schematized by color.



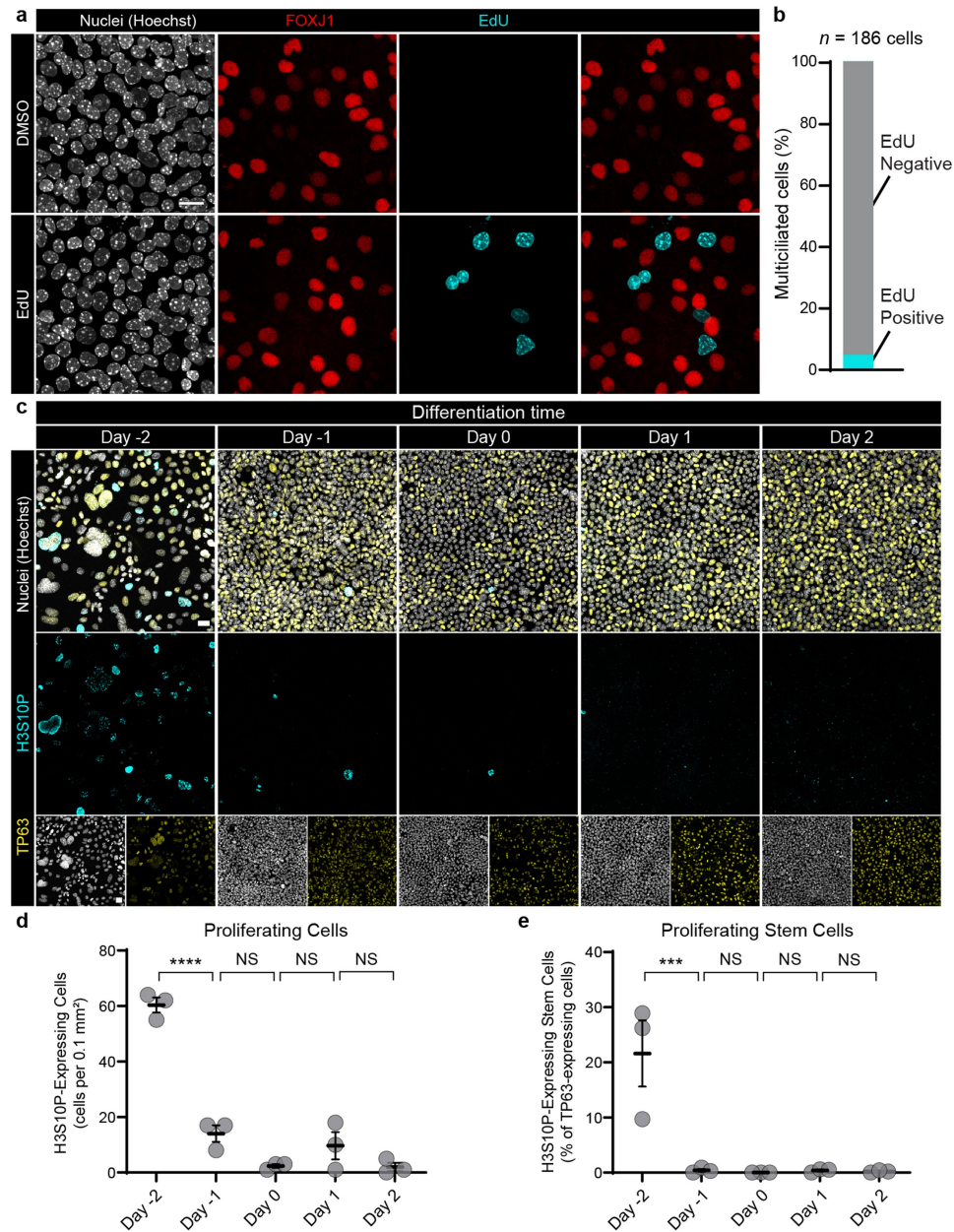
Extended Data Fig. 2 | A time course of mTEC differentiation captured by scRNA-seq reveals expression of cell cycle regulators. **a**, Integrated scRNA-seq dataset of mTECs on day 1, 3, 9, and 36 at air-liquid interface culture. Clusters are distinguished by color. **b**, Individual day 1, 3, 9, and 36 datasets that contribute to the integrated dataset. **c**, Expression of select marker genes for basal stem cells (*Krt5*), secretory cells (*Scgb3a1*), deuterosome-producing differentiating multiciliated cells (*Deup1*) and mature multiciliated cells

(*Dnah5*) overlaid on the UMAP of the integrated dataset. Color indicates expression level. **d**, Pseudotime values for proliferating basal stem cells. **e**, Pseudotime values for differentiating multiciliated cells. **f**, Heatmap of average expression of select cell cycle-related genes in both basal stem (above) and multiciliated (below) cells across S and G2/M-binned phases of the cell cycle. Color indicates expression (z-score).



Extended Data Fig. 3 | Differentiating multiciliated cells express cell cycle regulators and ciliogenesis genes. **a**, Heatmap of cell cycle and ciliogenesis genes arranged across multiciliated cell differentiation pseudotime. Color of individual boxes in heatmap indicates expression (z-score). S (blue) and G2/M (green) phase scores represent normalized expression of genes associated with each stage of the cell cycle. Select genes associated with cell cycle and

multiciliation functional categories are listed. Cluster identity of cells is schematized by color below. **b**, Average minimum and maximum normalized expression across multiciliated cell differentiation pseudotime of select genes encoding CDK proteins, cyclins, composite scores of S and G2/M phase-related genes, multiciliated cell transcription factors, proteins involved in centriole synthesis and maturation, or proteins involved in ciliogenesis.

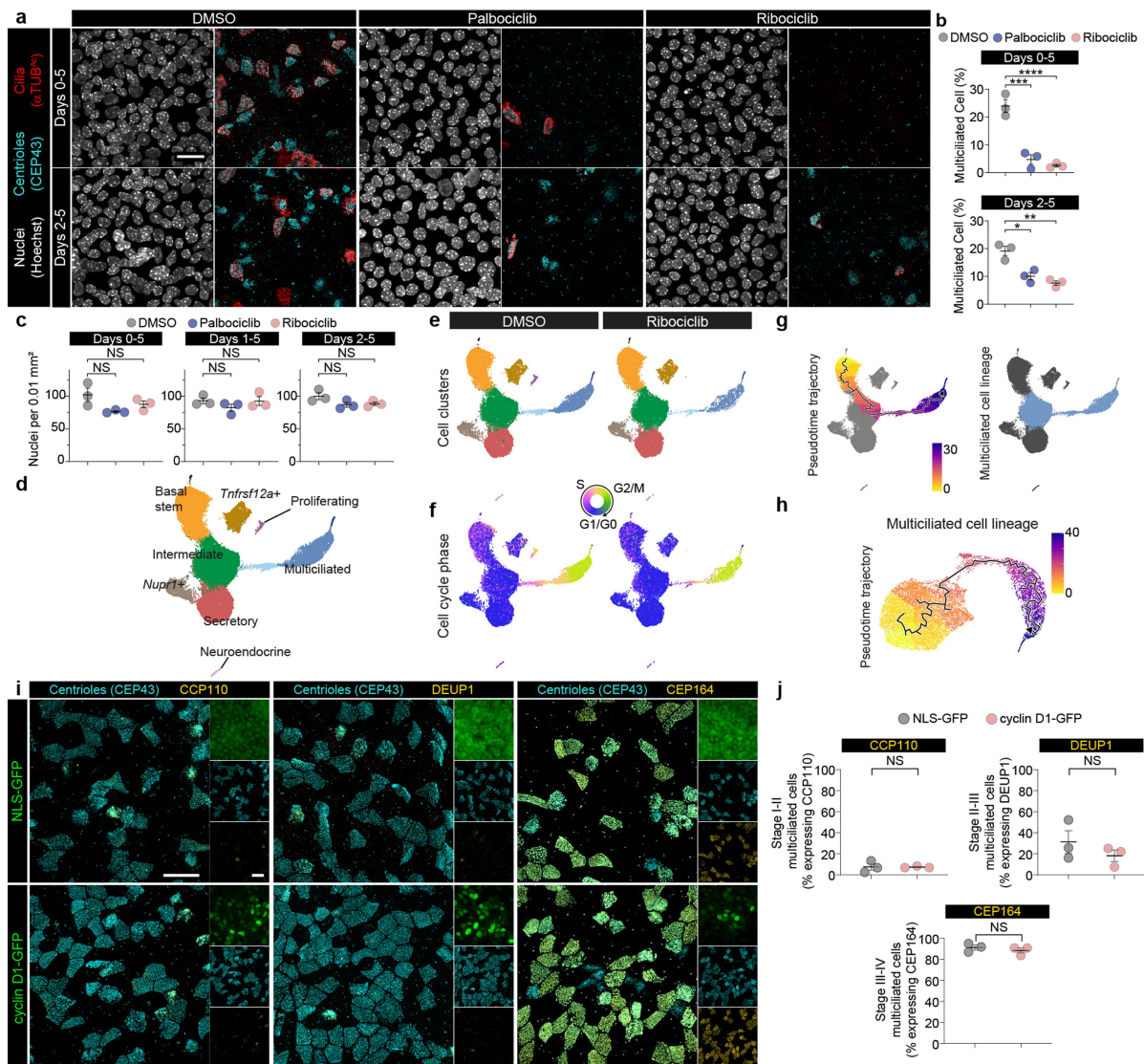


Extended Data Fig. 4 | mTECs cease proliferating during differentiation.

a, Representative immunofluorescence images of wild-type mTECs cultured at air-liquid interface for five days and stained for EdU (cyan), FOXJ1 (red) and nuclei (Hoechst, grey). EdU or DMSO was added during days one to five of culture at air-liquid interface. $n = 3$ biological replicates. Scale bar, 10 μ m.

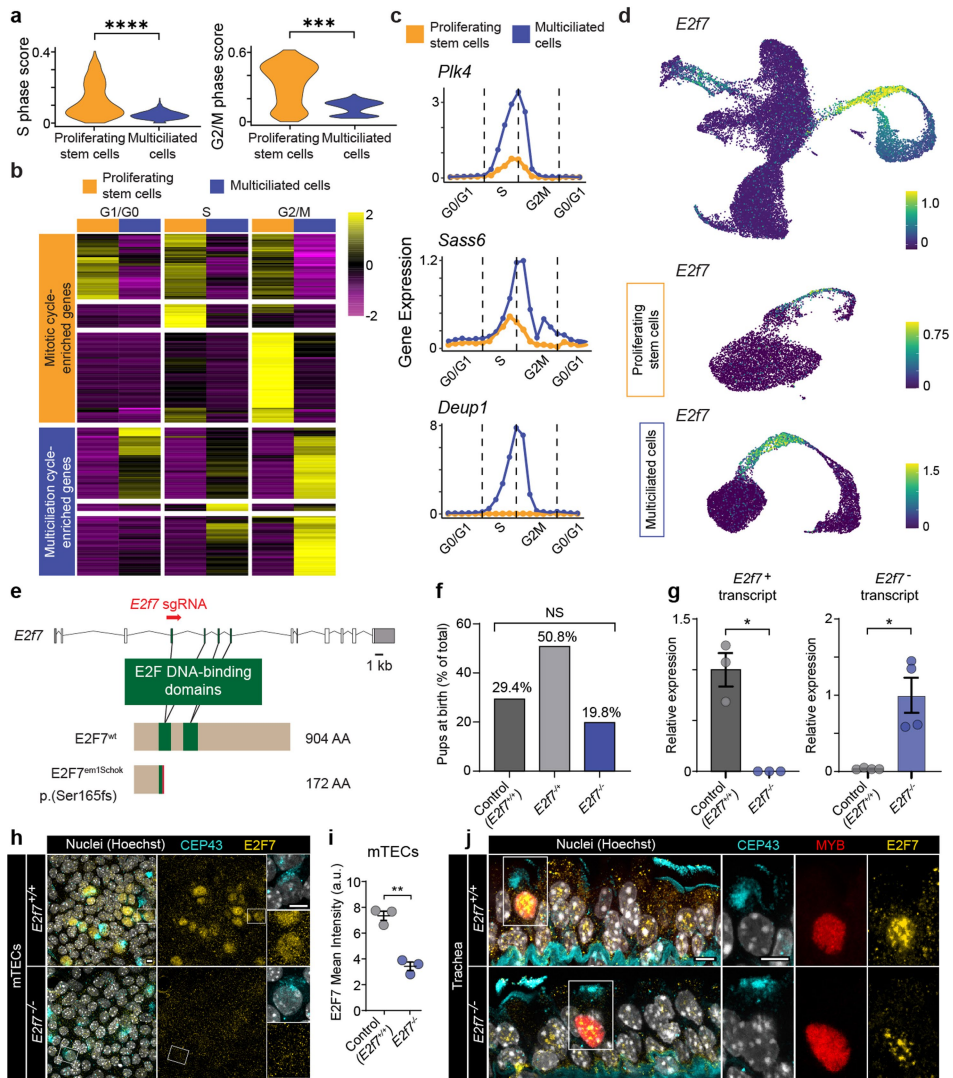
b, Percentage of multiciliated cells (expressing FOXJ1) that exhibit EdU incorporation. Bar graph quantitates EdU incorporation in 186 multiciliated cells assessed from 3 biological replicates. **c**, Immunofluorescence images of differentiating wild-type mTECs. mTECs were stained for Histone 3 phosphorylated at serine 10 (H3S10P, cyan), TP63 (yellow) and nuclei (Hoechst, grey) two days before transition to air-liquid interface (Day -2), one day before

(Day -1), the day of transition (Day 0), one day after transition to air-liquid interface (Day 1) or two days after (Day 2). H3S10P is a marker of cells in mitosis. TP63, also known as p63, is a marker of airway stem cells. Lower panels depict individual channels. Scale bar, 10 μ m. **d**, Percentage of H3S10P-expressing cells in differentiating mTECs at the indicated times. Horizontal lines indicate means \pm s.e.m. of 3 biological replicates, $****P = 0.000002$ and NS, not significant (one-way ANOVA with Sidak's correction). **e**, Percentage of TP63-expressing airway stem cells that also express H3S10P in differentiating mTECs at the indicated times. Horizontal lines indicate means \pm s.e.m. of 3 biological replicates, $***P = 0.0009$ and NS, not significant (one-way ANOVA with Sidak's correction).



Extended Data Fig. 5 | Assessment of roles of CDK4/6 and cyclin D1 in mTEC proliferation and differentiation. **a**, Immunofluorescence images of mTECs treated with DMSO, palbociclib or ribociclib during days 0–5 or days 2–5 at air–liquid interface and stained for centrioles (CEP43, cyan), cilia (αTub^{Ac}, red) and nuclei (grey). Scale bar, 10 μm. **b**, Percentage of multiciliated cells in mTECs treated with DMSO, palbociclib or ribociclib for given timepoints. Horizontal lines indicate means ± s.e.m. of 3 biological replicates, *** P = 0.0004, **** P = 0.0002, * P = 0.0059, ** P = 0.0018 (one-way ANOVA with Sidak's correction). **c**, Nuclear density of mTECs treated with DMSO, palbociclib or ribociclib for given timepoints. Horizontal lines indicate means ± s.e.m. of 3 biological replicates, NS, not significant (one-way ANOVA with Dunnett's correction). **d**, UMAP of integrated scRNA-seq data of DMSO- and ribociclib-treated mTECs. Clusters are distinguished by color. **e**, Individual scRNA-seq datasets of DMSO- or ribociclib-treated mTECs. Clusters are distinguished by color. **f**, Individual scRNA-seq datasets of DMSO- or ribociclib-treated mTECs

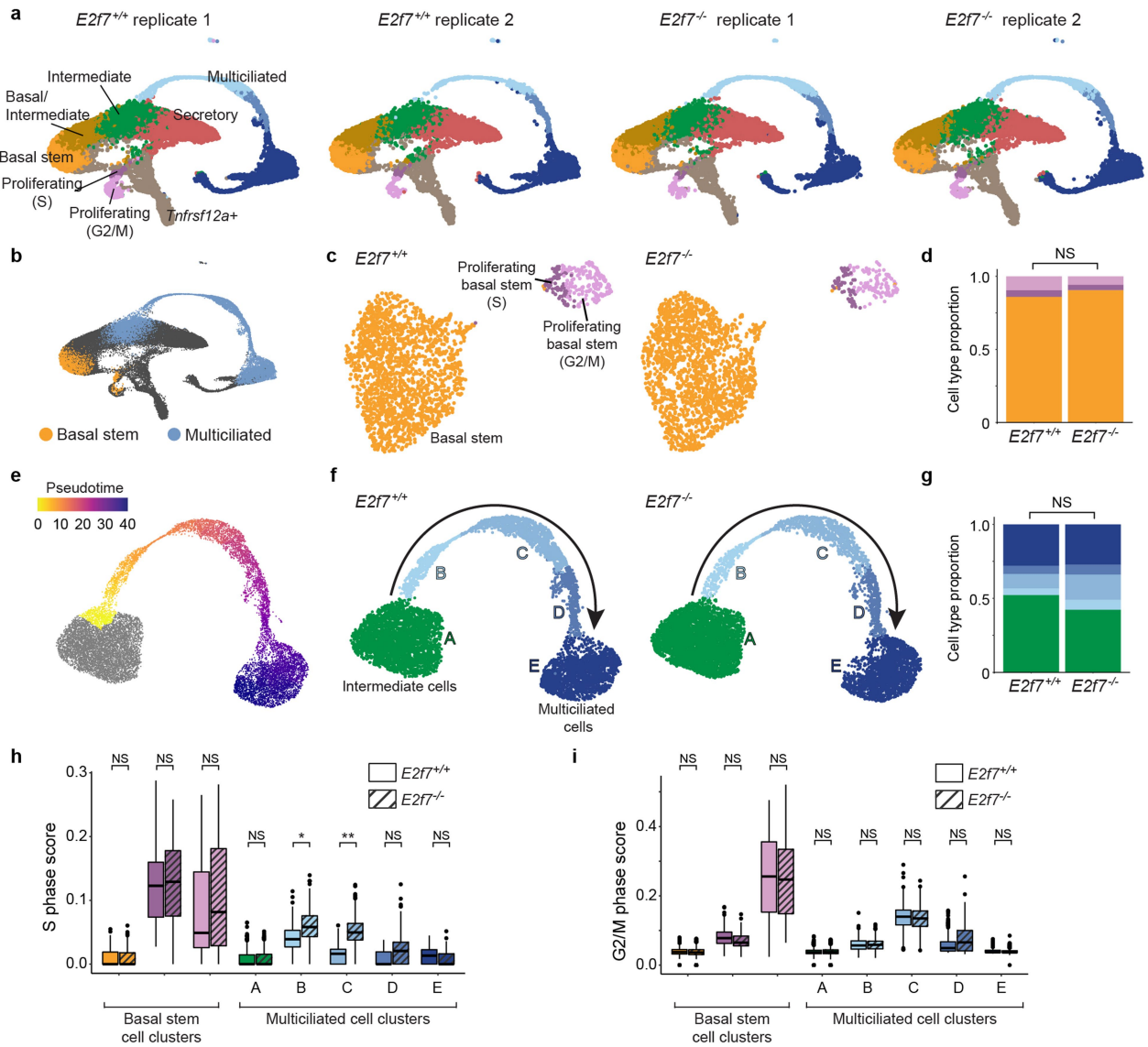
colored by cell cycle phase scores determined by tricycle analysis. **g**, Integrated scRNA-seq dataset with pseudotime values of cells of the basal stem, intermediate and multiciliated cell clusters. Pseudotime infers a differentiation trajectory (black arrow). Integrated scRNA-seq dataset with blue indicating cells expressing markers of intermediate and multiciliated cells (e.g., *Gmnc* and *Foxj1*) selected for subclustering and pseudotime analysis. **h**, Pseudotime values of cells of the intermediate and multiciliated cell clusters. Pseudotime infers a differentiation trajectory (black arrow). **i**, Immunofluorescence images of mTECs transduced with lentivirus expressing NLS-GFP (control) or cyclin D1-GFP and stained for centrioles (CEP43, cyan) and markers of multiciliated cell differentiation: CCP110, deuterosomes (DEUP1) and distal appendages (CEP164). Individual channels are shown to the right. Scale bars, 10 μm. **j**, Percentage of multiciliated cells expressing CCP110, DEUP1 or CEP164 in mTECs expressing NLS-GFP or cyclin D1-GFP. Horizontal lines indicate means ± s.e.m. of 3 biological replicates, NS, not significant (unpaired two-tailed *t*-test).



Extended Data Fig. 6 | Comparing transcriptional signatures of the canonical cell cycle and multiciliation cycle identifies E2f7. **a**, Proliferating stem (orange) and multililiated (blue) cells in S or G2/M phase scored for the expression of S or G2/M phase genes. Scores are normalized Mann-Whitney *U*-statistic of gene set expression. *****P* = 0.000002, ****P* = 0.00001 (unpaired two-tailed *t*-tests). **b**, Heatmap of cell cycle-related genes differentially expressed between proliferating stem and multililiated cells during each cell cycle phase. Color indicates expression (z-score). **c**, Average expression of select genes preferentially expressed during the multiciliation cycle across cycle phases of proliferating stem and multililiated cells. **d**, Expression of E2f7 projected onto the UMAP of the integrated mTEC dataset, proliferating stem and multililiated cell subset. Color indicates expression level. **e**, E2f7 mutation generation using an sgRNA (red arrow) homologous to mouse exon 4. The E2f7^{em1Sck} allele is predicted to generate a frameshift after codon 165 and referred to as E2f7⁻. Scale bar, 1 kb. **f**, Genotypes of offspring of intercrossed

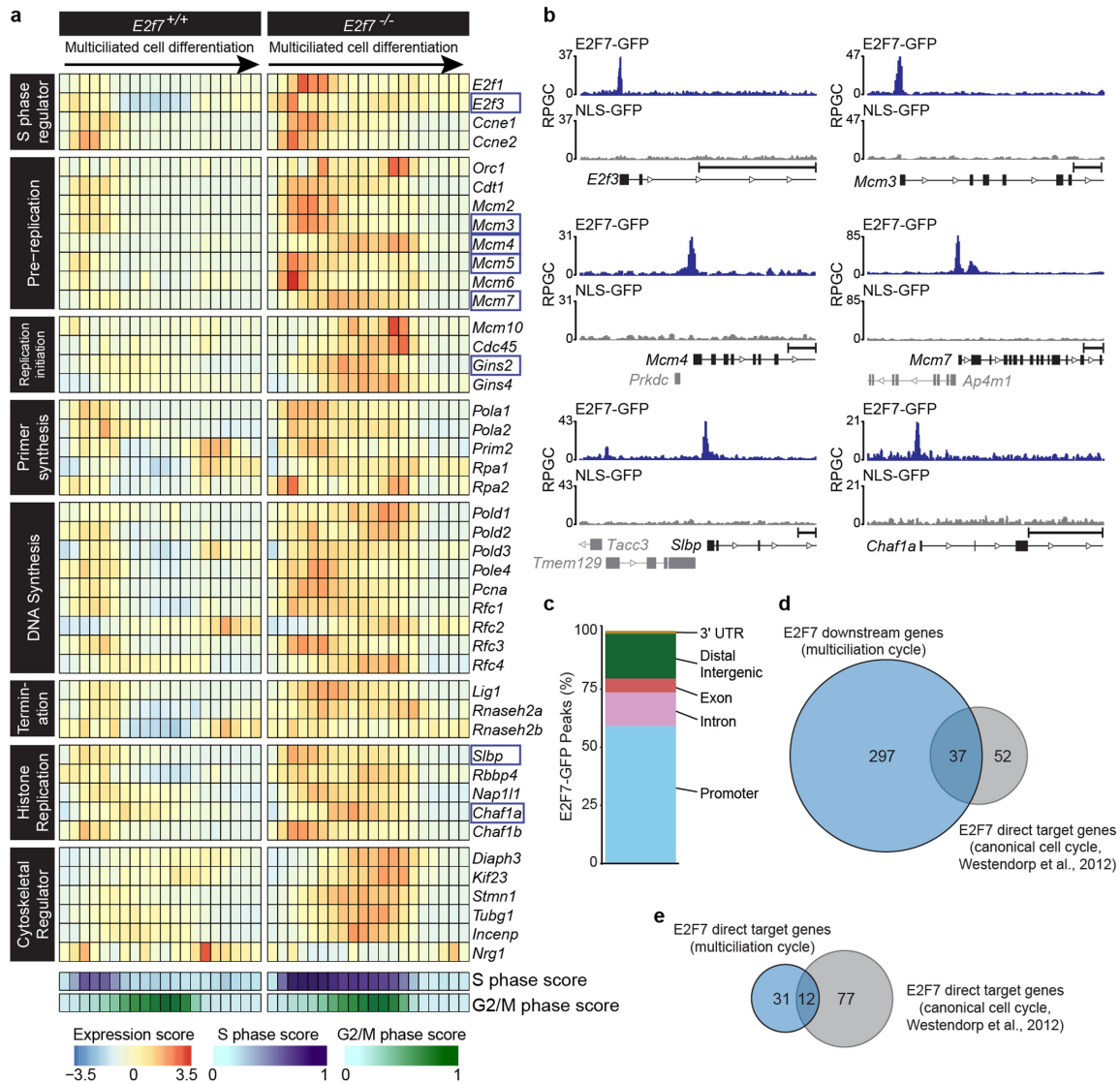
E2f7^{-/-} mice reveals no significant difference between observed and expected ratios (1E2f7^{+/+}:2E2f7^{+/+}:1E2f7^{-/-}, chi-squared test). *n* = 126 mice from 16 litters. **g**, Allele-specific (E2f7^{+/+} or E2f7^{-/-}) quantitative PCR on cDNA from E2f7^{+/+} or E2f7^{-/-} mTECs. Bars indicate means ± s.e.m. of 3 (E2f7^{+/+}) or 4 (E2f7^{-/-}) biological replicates. Points at value 0 indicate undetectable expression. **P* = 0.0259 (E2f7^{+/+}) or **P* = 0.0246 (E2f7^{-/-}) (paired two-tailed *t*-test). **h**, Immunofluorescence images of E2f7^{+/+} and E2f7^{-/-} mTECs stained for E2f7 (yellow), centrioles (CEP43, cyan) and nuclei (grey). Right: magnifications of boxed cells. Scale bars, 5 μm. **i**, E2f7 nuclear intensity in multililiated cells in E2f7^{+/+} and E2f7^{-/-} mTECs. Horizontal lines indicate means ± s.e.m. of 3 biological replicates, ***P* = 0.0013 (unpaired two-tailed *t*-test). **j**, Representative images of adult trachea from E2f7^{+/+} and E2f7^{-/-} mice immunostained for E2f7 (yellow), MYB (red), centrioles (CEP43, cyan) and nuclei (grey). Right: magnifications of boxed cells. *n* = 3 biological replicates. Scale bars, 10 μm.

Article



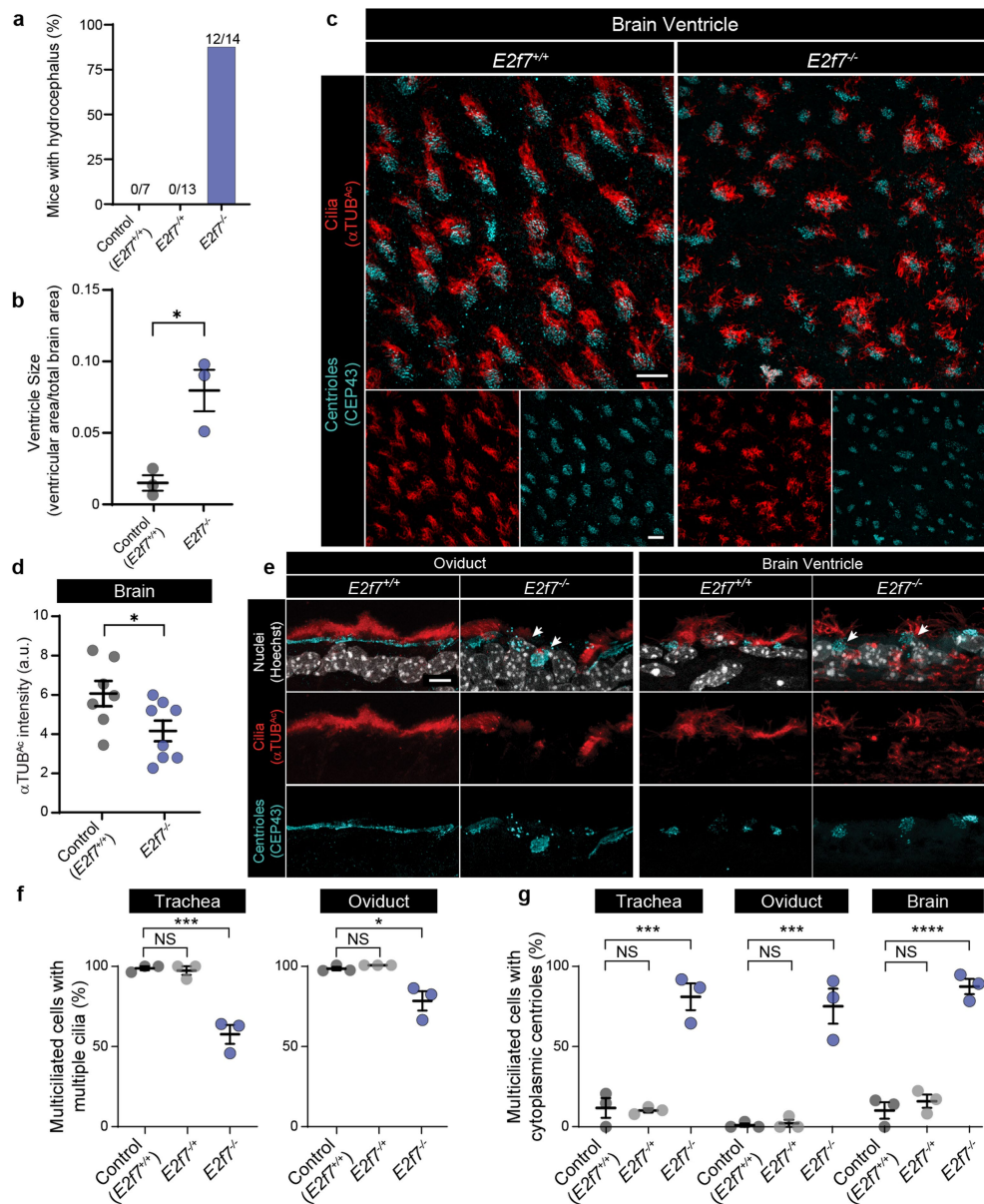
Extended Data Fig. 7 | E2F7 regulates S phase-like gene expression during multiciliated cell differentiation. **a**, Individual replicate scRNA-seq datasets of *E2f7^{+/+}* and *E2f7^{-/-}* mTECs after culture at air-liquid interface for seven days. Clusters are distinguished by color. **b**, Integrated scRNA-seq dataset of *E2f7^{+/+}* and *E2f7^{-/-}* mTECs with cells highlighted from which basal stem- (orange) and multiciliated- (blue) subclustered scRNA-seq datasets were derived (Fig. 3). **c**, Clusters of *E2f7^{+/+}* and *E2f7^{-/-}* mTEC-derived basal stem cells. Colors distinguish clusters. **d**, Proportion of basal stem cell clusters in *E2f7^{+/+}* and *E2f7^{-/-}* mTECs. Colors distinguish clusters, NS, not significant (two-tailed Moderated t-test with Benjamini-Hochberg correction). **e**, Pseudotime values across multiciliated cell differentiation. **f**, Clusters of *E2f7^{+/+}* and *E2f7^{-/-}* mTEC-derived multiciliated cells. Colors distinguish clusters, labeled A-E. Arrows indicate the inferred pseudotime differentiation trajectory. **g**, Proportion of multiciliated cell

clusters in *E2f7^{+/+}* and *E2f7^{-/-}* mTECs. Colors distinguish clusters A-E, NS, not significant (two-tailed Moderated t-test with Benjamini-Hochberg correction). **h**, Box plots depicting S phase gene signature scores of *E2f7^{+/+}* and *E2f7^{-/-}* basal stem and multiciliated cell clusters. Bars are colored by cluster. Boxes show interquartile range, horizontal bars indicate medians and whiskers show the minimum and maximum values of 2 biological replicates, with outliers plotted individually, *P = 0.0014, **P = 0.0013 (multiple unpaired t-tests with Holm-Sidak correction). **i**, Box plots depicting G2/M phase gene signature scores of *E2f7^{+/+}* and *E2f7^{-/-}* basal stem and multiciliated cell clusters. Bars are colored by cluster. Boxes show interquartile range, horizontal bars indicate medians and whiskers show the minimum and maximum values of 2 biological replicates, with outliers plotted individually, NS, not significant (multiple unpaired t-tests with Holm-Sidak correction).



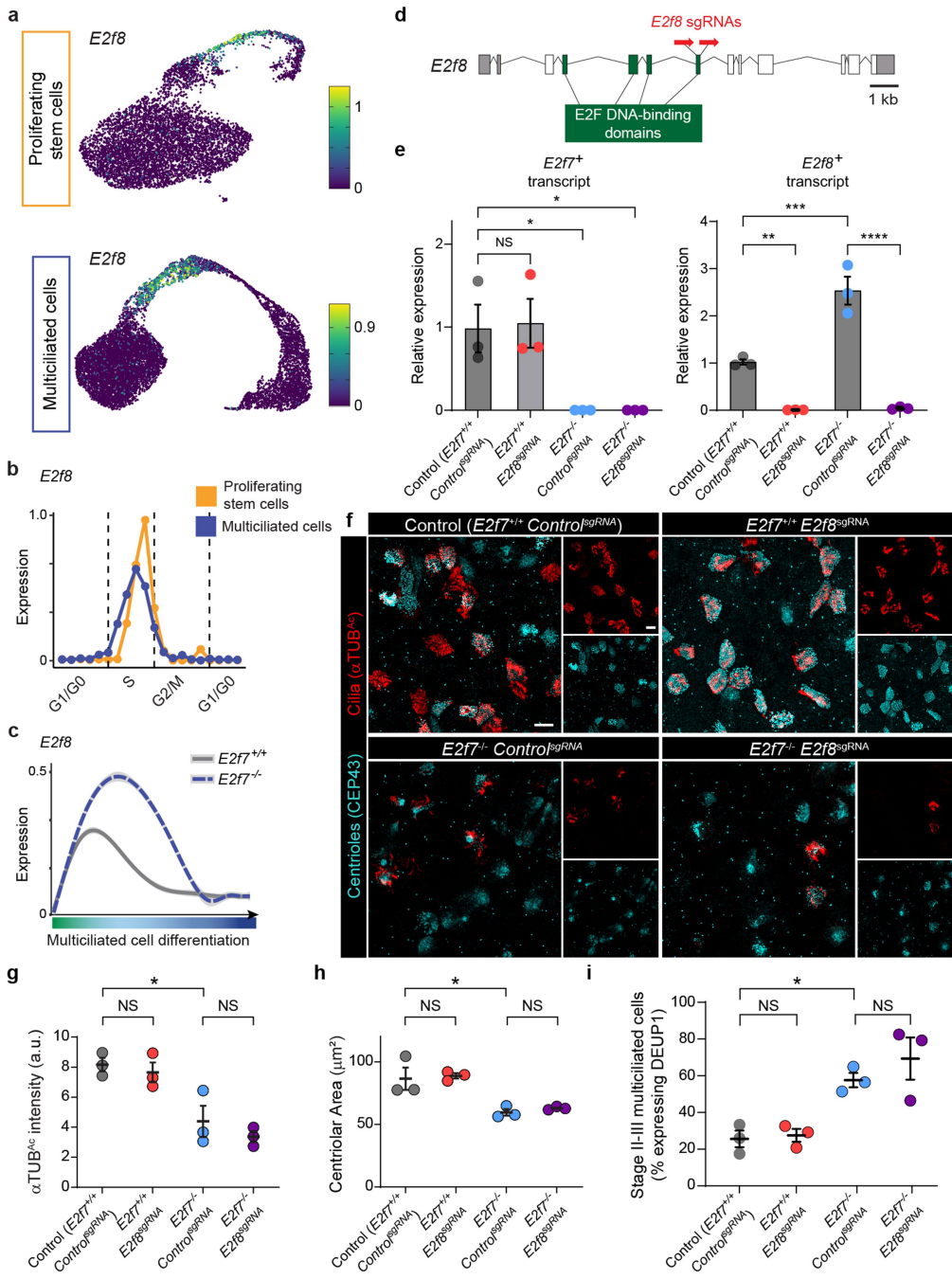
Extended Data Fig. 8 | E2F7 directly represses genes encoding DNA replication proteins. **a**, Heatmap of DNA replication-, S phase- and cytoskeleton-associated genes differentially expressed between *E2f7*^{+/+} and *E2f7*^{-/-} multiciliated cells derived from mTEC scRNA-seq data. Boxes represent bins of expression arranged across multiciliated cell differentiation pseudotime. Color indicates expression (z-score). S (blue) and G2/M (green) phase scores represent normalized expression of genes associated with each cell cycle phase. Genes near E2F7-GFP CUT&RUN peaks are outlined in blue. **b**, mTECs transduced with E2F7-GFP or a control (NLS-GFP) lentivirus were analyzed using CUT&RUN. CUT&RUN peaks for a subset of genes encoding DNA

replication machinery that are differentially expressed between *E2f7*^{+/+} and *E2f7*^{-/-} multiciliated cells are shown. y-axes represent reads per genomic content. Scale bars, 1 kb. **c**, Distribution of E2F7-GFP peaks relative to gene positions. **d**, Venn diagram of the overlap of the 334 genes differentially expressed between *E2f7*^{+/+} and *E2f7*^{-/-} multiciliated cells (blue) and 89 E2F7 direct target genes previously identified in proliferating cells by Westendorp et al.³⁴ (grey). **e**, Venn diagram of the overlap of the 43 genes near E2F7 CUT&RUN peaks in mTECs (blue) and 89 E2F7 direct target genes previously identified in proliferating cells by Westendorp et al.³⁴ (grey).

**Extended Data Fig. 9 |** **E2f7 is required for multiciliated cell differentiation.**

a. Hydrocephalus quantification of 34 progeny from 6 litters of $E2f7^{+/+}$ or $E2f7^{-/-}$ mice crossed with $E2f7^{-/-}$ mice. Fractions are the number of mice of each genotype with hydrocephalus over the total number of mice of that genotype assessed. **b.** Ratio of ventricle area to whole brain area in sections from adult $E2f7^{+/+}$ and $E2f7^{-/-}$ mice. Horizontal lines indicate means \pm s.e.m. of three different mice, * $P = 0.0139$ (unpaired two-tailed t -test). **c.** Brain ventricles of adult $E2f7^{+/+}$ and $E2f7^{-/-}$ mice immunostained for centrioles (CEP43, cyan) and cilia (α Tub $^{\text{Ac}}$, red). Right panels show individual channels. Scale bars, 10 μm . **d.** Quantitation of acetylated tubulin (α Tub $^{\text{Ac}}$) intensity in multiciliated cells of $E2f7^{+/+}$ and $E2f7^{-/-}$ brain ventricles. Each dot represents the mean α Tub $^{\text{Ac}}$ intensity of >100 multiciliated ependymal cells from a mouse brain, with $n = 7$ $E2f7^{+/+}$ mice and $n = 8$ $E2f7^{-/-}$ mice. Horizontal lines indicate means \pm s.e.m., * $P = 0.0381$ (unpaired two-tailed t -test).

* $P = 0.0381$ (unpaired two-tailed t -test). **e.** Sections of oviducts (left) or brain ventricles (right) of adult $E2f7^{+/+}$ and $E2f7^{-/-}$ mice immunostained for centrioles (CEP43, cyan), cilia (α Tub $^{\text{Ac}}$, red) and nuclei (Hoechst, gray). Lower panels show individual channels. White arrows indicate $E2f7^{-/-}$ cells with accumulated cytoplasmic centrioles. Scale bar, 10 μm . **f.** Percentages of cells with >5 centrioles that have multiple cilia in adult mouse tracheas and oviducts. Horizontal lines indicate means \pm s.e.m. of 3 mice, *** $P = 0.0005$ and * $P = 0.0142$ (ordinary one-way ANOVA with Sidak's correction). **g.** Percentages of multiciliated cells with centrioles undocked to the apical membrane in adult mouse tracheas, oviducts and brain ventricles. Horizontal lines indicate means \pm s.e.m. of 3 mice, *** $P = 0.0004$ and **** $P = 0.00005$ (ordinary one-way ANOVA with Sidak's correction).



Extended Data Fig. 10 | *E2f8* is dispensable for multiciliation. **a**, Expression of *E2f8* projected onto the UMAPs of basal stem and multiciliated cells from the mTEC timecourse scRNA-seq dataset. Color indicates expression level. **b**, Average expression of *E2f8* across cycle phases of basal stem and multiciliated cells. **c**, scRNA-seq expression of *E2f8* in *E2f7^{+/+}* and *E2f7^{-/-}* across differentiation pseudotime. Grey bars indicate 95% confidence intervals. Colors indicate cluster identity. **d**, Strategy for generating *E2f8* knockout mTECs. Red arrows indicate positions of sgRNAs homologous to sequences in exon 7 of *E2f8*. Scale bar, 1 kb. **e**, Quantitative RT-PCR for wild-type *E2f7* (*E2f7^{+/+}*) and *E2f8* (*E2f8^{+/+}*) transcripts from control (*E2f7^{+/+} Control^{sgRNA}*), *E2f7* mutant (*E2f7^{+/+} E2f8^{sgRNA}*), *E2f7^{-/-}* (*E2f7^{-/-} Control^{sgRNA}*) or *E2f7* and *E2f8* double mutant (*E2f7^{-/-} E2f8^{sgRNA}*) mTECs. Bars indicate means \pm s.e.m. of 3 biological replicates. Points at value 0 indicate undetectable expression. * $P = 0.0284$, ** $P = 0.0043$, *** $P = 0.00003$, **** $P = 0.000008$ (one-way ANOVA with Sidak's correction). **f**, Immunofluorescence images of control, *E2f8* mutant, *E2f7*

mutant, or *E2f7* and *E2f8* double mutant mTECs cultured for 7 days at air-liquid interface, stained for centrioles (CEP43, cyan) and cilia (α Tub^{Ac}, red). Right: individual channels. Scale bars, 10 μ m. **g**, α Tub^{Ac} intensity in control, *E2f7* mutant, *E2f7* mutant, and *E2f7* and *E2f8* double mutant mTECs cultured for 7 days at air-liquid interface. Horizontal lines indicate means \pm s.e.m. of 3 biological replicates, * $P = 0.0130$ (one-way ANOVA with Sidak's correction). **h**, Centriolar area in control, *E2f8* mutant, *E2f7* mutant, and *E2f7* and *E2f8* double mutant mTECs cultured for 7 days at air-liquid interface. Horizontal lines indicate means \pm s.e.m. of 3 biological replicates * $P = 0.0121$ (one-way ANOVA with Sidak's correction). **i**, Percentage of control, *E2f8* mutant, *E2f7* mutant, and *E2f7* and *E2f8* double mutant multiciliated cells containing deuterosomes (DEUP1) in mTECs cultured for 7 days at air-liquid interface. Horizontal lines indicate means \pm s.e.m. of 3 biological replicates * $P = 0.0295$ (one-way ANOVA with Sidak's correction).

Reporting Summary

Nature Portfolio wishes to improve the reproducibility of the work that we publish. This form provides structure for consistency and transparency in reporting. For further information on Nature Portfolio policies, see our [Editorial Policies](#) and the [Editorial Policy Checklist](#).

Statistics

For all statistical analyses, confirm that the following items are present in the figure legend, table legend, main text, or Methods section.

n/a Confirmed

- The exact sample size (n) for each experimental group/condition, given as a discrete number and unit of measurement
- A statement on whether measurements were taken from distinct samples or whether the same sample was measured repeatedly
- The statistical test(s) used AND whether they are one- or two-sided
Only common tests should be described solely by name; describe more complex techniques in the Methods section.
- A description of all covariates tested
- A description of any assumptions or corrections, such as tests of normality and adjustment for multiple comparisons
- A full description of the statistical parameters including central tendency (e.g. means) or other basic estimates (e.g. regression coefficient) AND variation (e.g. standard deviation) or associated estimates of uncertainty (e.g. confidence intervals)
- For null hypothesis testing, the test statistic (e.g. F , t , r) with confidence intervals, effect sizes, degrees of freedom and P value noted
Give P values as exact values whenever suitable.
- For Bayesian analysis, information on the choice of priors and Markov chain Monte Carlo settings
- For hierarchical and complex designs, identification of the appropriate level for tests and full reporting of outcomes
- Estimates of effect sizes (e.g. Cohen's d , Pearson's r), indicating how they were calculated

Our web collection on [statistics for biologists](#) contains articles on many of the points above.

Software and code

Policy information about [availability of computer code](#)

Data collection ZEN Microscopy Software v3.7 (Zeiss)

Data analysis Prism v9.5.1 (GraphPad)
QuantStudio Design & Analysis Software v1.5.1 (appliedbiosystems)
ImageJ v1.53c (NIH)
ICE Analysis v3.0 (Synthego)
The following software packages and code were used for scRNA-seq and CUT&RUN analyses. References for all software packages are included in the methods:
CellRanger v3.0, v7.0 and v7.1
Scrublet v0.2.1
DoubletFinder v2.0
SoupX v1.5.0
Seurat v4
Monocle3 v1.2
Speckle v0.99.7
edgeR v3.40.2
Tricycle v1.6.0
UCell v2.2.0
DESeq2 v1.38.3
trimmomatic v0.39
bowtie2 v2.4.2

samtools v1.10
picard v2.24.0
MACS2 v2.1.2
ChIPseeker v1.34.1
ggplot2 v3.4.2

For manuscripts utilizing custom algorithms or software that are central to the research but not yet described in published literature, software must be made available to editors and reviewers. We strongly encourage code deposition in a community repository (e.g. GitHub). See the Nature Portfolio [guidelines for submitting code & software](#) for further information.

Data

Policy information about [availability of data](#)

All manuscripts must include a [data availability statement](#). This statement should provide the following information, where applicable:

- Accession codes, unique identifiers, or web links for publicly available datasets
- A description of any restrictions on data availability
- For clinical datasets or third party data, please ensure that the statement adheres to our [policy](#)

scRNA-seq and CUT&RUN raw FASTQ files and processed data have been deposited in the Gene Expression Ombibus (GEO) under accession GSE228110. scRNA-seq datasets have been deposited in the CellxGene single cell browser at <https://cellxgene.cziscience.com/collections/c26ca66a-63ea-4059-a24e-0e0be0a2a173>. The mouse mm10 reference genome was downloaded for analysis and is available at <https://www.10xgenomics.com/support/software/cell-ranger/downloads/cr-ref-build-steps#mouse-ref-3-0-0-mm10-vdj>.

Research involving human participants, their data, or biological material

Policy information about studies with [human participants or human data](#). See also policy information about [sex, gender \(identity/presentation\), and sexual orientation](#) and [race, ethnicity and racism](#).

Reporting on sex and gender

n/a

Reporting on race, ethnicity, or other socially relevant groupings

n/a

Population characteristics

n/a

Recruitment

n/a

Ethics oversight

n/a

Note that full information on the approval of the study protocol must also be provided in the manuscript.

Field-specific reporting

Please select the one below that is the best fit for your research. If you are not sure, read the appropriate sections before making your selection.

Life sciences Behavioural & social sciences Ecological, evolutionary & environmental sciences

For a reference copy of the document with all sections, see nature.com/documents/nr-reporting-summary-flat.pdf

Life sciences study design

All studies must disclose on these points even when the disclosure is negative.

Sample size

Sample size was determined by assessing previously published experiments and adhering to standards in the field (PMID: 24048590, PMID: 27257214, PMID: 24240477, PMID: 30152757). For most experiments a minimum of n =3 independently derived mouse tracheal epithelial cells (mTECs) was measured. Specific sample sizes are provided in each figure legend or in the Methods.

Data exclusions

No data were excluded from imaging experiments. For scRNA-seq datasets, individual cells that did not meet thresholds for percent mitochondrial reads and number of genes per cell were removed. Thresholds were determined by the histogram distribution of each measurement for each individual dataset. Thresholds used for each dataset are available on github (https://github.com/lb15/multiciliation_cycle/) as a parameter file (parameters.csv) associated with each dataset. Cells identified as doublets by Scrublet were removed. If a cluster contained greater than 15% (E2f7-focused dataset) or 50% (time course-focused dataset) identified doublets, all cells

from that cluster were removed. After integration of individual datasets, in both the time course and E2f7-focused datasets, a subcluster of mature multiciliated cells shared gene expression with other gene types and was removed from further analysis.

Replication	All reported findings were successfully replicated in two additional biological samples unless otherwise indicated in the Methods. Biological replicate number for each experiment is given in the accompanying legend.
Randomization	For mouse experiments, mice of each genotype were randomly assigned to each experiment. For mTEC experiments, mice were randomly assigned to each preparation of primary stem cells. For all treatments (small molecule or lentiviral), transwells containing primary stem cells were randomly assigned to each group.
Blinding	No blinding of samples was performed because perturbations (either genetic, lentiviral or small molecule) were readily identified by cell morphology or centriolar/ciliary distribution. To reduce bias, quantitative measurements were made for most experiments.

Reporting for specific materials, systems and methods

We require information from authors about some types of materials, experimental systems and methods used in many studies. Here, indicate whether each material, system or method listed is relevant to your study. If you are not sure if a list item applies to your research, read the appropriate section before selecting a response.

Materials & experimental systems		Methods	
n/a	Involved in the study	n/a	Involved in the study
<input type="checkbox"/>	<input checked="" type="checkbox"/> Antibodies	<input type="checkbox"/>	<input checked="" type="checkbox"/> ChIP-seq
<input type="checkbox"/>	<input checked="" type="checkbox"/> Eukaryotic cell lines	<input checked="" type="checkbox"/>	<input type="checkbox"/> Flow cytometry
<input checked="" type="checkbox"/>	<input type="checkbox"/> Palaeontology and archaeology	<input checked="" type="checkbox"/>	<input type="checkbox"/> MRI-based neuroimaging
<input type="checkbox"/>	<input checked="" type="checkbox"/> Animals and other organisms		
<input checked="" type="checkbox"/>	<input type="checkbox"/> Clinical data		
<input checked="" type="checkbox"/>	<input type="checkbox"/> Dual use research of concern		
<input checked="" type="checkbox"/>	<input type="checkbox"/> Plants		

Antibodies

Antibodies used	alphaTUBAc (Mouse, Sigma-Aldrich, #T6793, Clone 6-11B-1) FGFR1OP (CEP43) (Rabbit, Proteintech, #11343-1-AP) FOP (CEP43) (Mouse, Abnova, #H00011116-M01, Clone 2B1) MYB (Rat, Abcam, #ab169111) FOXJ1 (Mouse, Thermo Fisher, #14-9965-82, Clone 2A5) E2F7 (Rabbit, Atlas Antibodies, #HPA064866) CCP110 (Rabbit, Proteintech, #12780-1-AP) DEUP1 (Rabbit, Sigma-Aldrich, #HPA010986) CEP164 (Rabbit, Zhu lab (Gift), PMID: 33627667) Cyclin D1 (Rabbit, Abcam, #ab16663) CDK1 (Rabbit, Sigma, #HPA003387) Cyclin B1 (Rabbit, Cell Signaling Technology, #4138) H3S10P (Rabbit, Cell Signaling Technology, #9701) TP63 (Mouse, Santa Cruz, #sc-8431, Clone 4A4) GFP (Rabbit, Abcam, #ab290) anti-Rat-AlexaFluor647 (Donkey, Abcam, #ab150151) anti-Rabbit-AlexaFluor488 (Donkey, Invitrogen, #A21206) anti-Rabbit-AlexaFluor568 (Donkey, Invitrogen, #A10042) anti-Rabbit-AlexaFluor647 (Donkey, Invitrogen, #A31573) anti-Mouse-AlexaFluor488 (Donkey, Invitrogen, #A21202) anti-Mouse-AlexaFluor568 (Donkey, Invitrogen, #A10037) anti-Mouse-AlexaFluor647 (Donkey, Invitrogen, #A31571) anti-Rabbit IgG (Guinea Pig, Rockland, #611-201-122)
-----------------	---

Validation	alphaTUBAc - Validated by western blot of purified protein with and without acetylation (PMID: 2415535) FGFR1OP (CEP43, Rabbit) - Knockdown validated (PMID: 30538248) FOP (CEP43, Mouse) - Overexpression validated by manufacturer (abnova.com) MYB - Knockout validated by manufacturer (abcam.com) FOXJ1 - Knockout validated by manufacturer (thermofisher.com) E2F7 - Knockout validated (this study, Extended Data Fig. 6h-j) CCP110 - Knockdown validated (PMID: 28385950) DEUP1 - Overexpression validated (PMID: 22610074) CEP164 - Validated by immunofluorescence with and without centrioles (PMID: 30833343) Cyclin D1 - Knockout validated by manufacturer (abcam.com) CDK1 - Validated by RNA expression correlation across tissues by manufacturer (atlasantibodies.com) Cyclin B1 - Validated by reduced CyclinB1 RNA levels following viral infection (PMID: 24415942) H3S10P (Rabbit, Cell Signaling Technology, #9701) - Validated by overexpression and blocking modification by manufacturer
------------	---

(cellsignal.com)
 TP63 (Mouse, Santa Cruz, #sc-8431) - Knockdown validated (PMID:21930775)
 GFP (Rabbit, Abcam, #ab290) - Overexpression validated (PMID: 36293380)
 anti-Rat-AlexaFluor647 (Donkey, Abcam, #ab150151) - Validated by immunofluorescence with no primary antibody control by manufacturer (abcam.com)
 anti-Rabbit-AlexaFluor488 (Donkey, Invitrogen, #A21206) - Validated by immunofluorescence with isotype and no primary antibody controls by manufacturer (thermofisher.com)
 anti-Rabbit-AlexaFluor568 (Donkey, Invitrogen, #A10042) - Validated by immunofluorescence with isotype and no primary antibody controls by manufacturer (thermofisher.com)
 anti-Rabbit-AlexaFluor647 (Donkey, Invitrogen, #A31573) - Validated by immunofluorescence with negative model (cell line) and no primary antibody controls by manufacturer (thermofisher.com)
 anti-Mouse-AlexaFluor488 (Donkey, Invitrogen, #A21202) - Validated by immunofluorescence with isotype and no primary antibody controls by manufacturer (thermofisher.com)
 anti-Mouse-AlexaFluor568 (Donkey, Invitrogen, #A10037) - Validated by immunofluorescence with isotype and no primary antibody controls by manufacturer (thermofisher.com)
 anti-Mouse-AlexaFluor647 (Donkey, Invitrogen, #A31571) - Validated by immunofluorescence with isotype and no primary antibody controls by manufacturer (thermofisher.com)
 anti-Rabbit IgG (Guinea Pig, Rockland, #611-201-122) - Validated by ELISA titration by manufacturer (rockland.com)

Eukaryotic cell lines

Policy information about [cell lines and Sex and Gender in Research](#)

Cell line source(s)	Lenti-X 293T (HEK293T) cells from Takara were used for lentivirus production
Authentication	Cells were purchased directly from the manufacturer, Takara, and were not independently authenticated beyond the identity provided.
Mycoplasma contamination	All cell lines tested negative for mycoplasma.
Commonly misidentified lines (See ICLAC register)	No commonly misidentified cell lines were used in this study.

Animals and other research organisms

Policy information about [studies involving animals; ARRIVE guidelines](#) recommended for reporting animal research, and [Sex and Gender in Research](#)

Laboratory animals	Wildtype mice (C57BL/6J) were used for most experiments in this study. To generate E2f7 knockout mice, injections were performed into zygotes from CD-1 female mice. All further breedings were performed to C57BL/6J mice to generate heterozygous mutant lines. All experiments were performed on adult mice (2-5 months old). C57BL/6J mice were obtained from Jackson Labs (JAX Stock #000664).
Wild animals	This study did not involve wild animals.
Reporting on sex	For all mTEC experiments, cells were derived from a balance of adult female and male mice. For mouse experiments, sex was tracked in order to ensure a balance of males and females in each experiment.
Field-collected samples	This study did not involve samples collected from the field.
Ethics oversight	Mice were housed under standard pathogen-free conditions at the University of California San Francisco animal care facility in the CVRI. All animal protocols and procedures were approved by the Institutional Animal Care and Use Committee (IACUC) of UCSF. Wild-type adult mice used in these studies were of the strain C57BL/6J, unless otherwise noted, and obtained from Jackson Labs (JAX Stock #000664). Mice were maintained in the CVRI vivarium (UCSF) under a 12 hour light, 12 hour dark cycle, at 30-70% humidity and at a temperature of 68-79°F.

Note that full information on the approval of the study protocol must also be provided in the manuscript.

Plants

Seed stocks	Report on the source of all seed stocks or other plant material used. If applicable, state the seed stock centre and catalogue number. If plant specimens were collected from the field, describe the collection location, date and sampling procedures.
Novel plant genotypes	Describe the methods by which all novel plant genotypes were produced. This includes those generated by transgenic approaches, gene editing, chemical/radiation-based mutagenesis and hybridization. For transgenic lines, describe the transformation method, the number of independent lines analyzed and the generation upon which experiments were performed. For gene-edited lines, describe the editor used, the endogenous sequence targeted for editing, the targeting guide RNA sequence (if applicable) and how the editor was applied.
Authentication	Describe any authentication procedures for each seed stock used or novel genotype generated. Describe any experiments used to assess the effect of a mutation and, where applicable, how potential secondary effects (e.g. second site T-DNA insertions, mosaicism, off-target gene editing) were examined.

ChIP-seq

Data deposition

- Confirm that both raw and final processed data have been deposited in a public database such as [GEO](#).
- Confirm that you have deposited or provided access to graph files (e.g. BED files) for the called peaks.

Data access links

May remain private before publication.

CUT&RUN raw FASTQ files and processed data are available on GEO as GSE228110.

Files in database submission

E2f7_A_S2_R1_001.fastq.gz
 E2f7_A_S2_R2_001.fastq.gz
 E2f7_B_S4_R1_001.fastq.gz
 E2f7_B_S4_R2_001.fastq.gz
 nlsGFP_A_S1_R1_001.fastq.gz
 nlsGFP_A_S1_R2_001.fastq.gz
 nlsGFP_B_S3_R1_001.fastq.gz
 nlsGFP_B_S3_R2_001.fastq.gz
 E2f7_A_henikoff_dupmark_120bp_RPGC.bw
 E2f7_A_vs_nlsGFP_A_dupmark_peaks.narrowPeak
 E2f7_B_henikoff_dupmark_120bp_RPGC.bw
 E2f7_B_vs_nlsGFP_B_dupmark_peaks.narrowPeak
 nlsGFP_A_henikoff_dupmark_120bp_RPGC.bw
 nlsGFP_B_henikoff_dupmark_120bp_RPGC.bw

Genome browser session (e.g. [UCSC](#))

Genome browser session: http://genome.ucsc.edu/s/Lb13/E2f7_CUTRUN

Methodology

Replicates

Two biological replicates from two independent mTEC preparations. Final peak list was produced by the intersection of both replicates.

Sequencing depth

Samples underwent paired-end sequencing of 42 bp read lengths, resulting in between 32-40 million reads/sample and uniquely mapped alignment rates of 66-67%.

Antibodies

Rabbit anti-GFP. Catalog # ab290 (Abcam)

Peak calling parameters

Reads were aligned with bowtie2 using parameters --local --very-sensitive-local --no-unal --no-mixed --no-discordant --phred33 -I 10 -X 700. Samples were filtered for reads under 120bp and duplicates were marked, but not removed, with picard MarkDuplicates. MACS2 was used to call peaks, using the callpeak command with parameters -g m --keep-dup all -f BAMPE -q 0.05 -B --SPMR and -c with the corresponding control being the NLS-GFP sample.

Data quality

Data quality was checked by alignment rate and duplication rate of individual libraries. The final peak list was generated from peaks only present in both replicates.

Software

Scripts were derived from CUT&RUNtools and scripts detailed here <https://www.protocols.io/view/cut-and-tag-data-processing-and-analysis-tutorial-e6nvw93x7gmk/v1>. Scripts are available at https://github.com/lb15/multiciliation_cycle. Scripts and R objects used for analysis are deposited at Zenodo <https://doi.org/10.5281/zenodo.10896100>. CUT&RUN analysis scripts are at <https://doi.org/10.5281/zenodo.10896066> and Seurat analysis scripts are at <https://doi.org/10.5281/zenodo.10896071>.